

## ABSTRACT

### Petrophysical Facies Mapping of the Pennsylvanian Cline Shale, Midland Basin, West Texas

Kieron C. Prince, M.S.

Thesis Chairperson: Stacy C. Atchley, Ph.D.

The Cline Shale is a Pennsylvanian unconventional shale resource play located in the Midland Basin, west Texas. This study evaluates the depositional, stratigraphic and petrologic controls on Cline Shale reservoir quality and their spatial distribution as determined from core-calibrated petrophysical facies across the study area. Eight depositional facies were observed and described from the cored Gunn36 #1 well located in Howard County. Five petrophysical facies were derived from the statistical comparison of core observed depositional facies with corresponding digital well log data. Two additional petrophysical facies that are not calibrated to core observations account for both the distribution of undifferentiated shallow-marine carbonates across the Horseshoe Atoll, and borehole washouts. By mapping the petrophysical facies, it was determined that the distribution of the most prospective Organic Rich Shale (ORS) facies, located principally in southwest Howard and northeast Glasscock counties, was controlled by proximity to the contemporaneous Horseshoe Atoll and Eastern Shelf.

Petrophysical Facies Mapping of the Pennsylvanian Cline Shale,  
Midland Basin, West Texas

by

Kieron C. Prince, B.S.

A Thesis

Approved by the Department of Geology

---

Stacy C. Atchley, Ph.D., Chairperson

Submitted to the Graduate Faculty of  
Baylor University in Partial Fulfillment of the  
Requirements for the Degree  
of  
Master of Science

Approved by the Thesis Committee

---

Stacy C. Atchley, Ph.D., Chairperson

---

Steven G. Driese, Ph.D.

---

Mark F. Taylor, Ph.D.

Accepted by the Graduate School

August 2015

---

J. Larry Lyon, Ph.D., Dean

Copyright © 2015 by Kieron C. Prince

All rights reserved

## TABLE OF CONTENTS

List of Tables	viii
Acknowledgments	ix
Chapter One	1
Introduction	1
Chapter Two	5
Paleogeography and Regional Stratigraphy	5
Midland Basin	5
Eastern Shelf	7
Lithostratigraphy	7
Chapter Three	10
Methods	10
Stratigraphic Correlation	10
Core Description	13
Facies Predictions	13
Structure Maps	14
Facies Maps	15
Chapter Four	16

Observed Facies and Environments	16
Black Laminated Mudrock - BLM	18
Mottled Black Mudrock - MBM	18
Skeletal Black Mudrock - SBM	20
Laminated Carbonate Mudstone - LCM	20
Mud Supported Carbonate - MSC	21
Grain Supported Carbonate - GSC	21
Lithoclastic Carbonate Floatstone - LCF	22
Inversely Graded Carbonate - IGC	22
Petrophysical Facies Description	23
Shallow Marine Carbonate - SMC	23
Wash-Out Zone - WOZ	24
Chapter Five	26
Distribution of Reservoir Quality	26
Chapter Six	35
Depositional History	35
Chapter Seven	38
Conclusions	38
Appendices	40
Appendix A: Structure Maps	41

Upper Strawn (Lower Lime) structure map	42
Three Fingers structure map	43
Cline Top structure map	44
Appendix B: Facies Isopach Maps	45
Cline interval isopach map	46
DCB facies isopach map	47
MCM facies isopach map	48
ORS/All other facies ratio isopach map	49
SMC facies isopach map	50
ORS/NRS facies ratio isopach map	51
Shale facies total/CGF facies ratio map	52
Shale facies total isopach map	53
Appendix C: Cross Sections	54
Appendix D: Core Descriptions	61
Appendix E: Digital Appendix:	Pocket in back
Manuscript (word document and PDF)	
Manuscript Figures (PNG and Canvas format)	
Core Photographs (JPEG format)	
Scanned Core Description Forms (Core description legend and forms in Canvas format)	
References	73

## LIST OF FIGURES

1. Paleogeography of the Late Pennsylvanian midcontinent seaway and location map.	2
2. Tobosa Basin extent map.	3
3. Pennsylvanian paleogeography and major structural features of the Permian Basin.	6
4. Stratigraphic correlation chart.	9
5. Cross section and location of cored well basemap.	11
6. Type log denoting stratigraphic tops.	12
7. Representative core photographs of observed facies.	19
8. Petrophysical facies and their gamma ray and density porosity parameters, and observed facies proportions.	25
9. Comparison of the Passey and Schmoker methods of TOC estimation with core-derived laboratory TOC measurements.	27
10. Box and whisker plot of depositional facies versus Schmoker-derived TOC estimates.	28
11. Box and whisker plot of petrophysical facies versus Schmoker-derived TOC estimates.	29
12. ORS facies isopach map.	30
13. NRS facies isopach map.	31
14. CGF facies isopach map.	33
15. ORS/CGF facies ratio isopach map.	34
16. Simplified A-A' cross section.	37

## LIST OF TABLES

- |                                      |    |
|--------------------------------------|----|
| 1. Guidelines for facies prediction. | 14 |
| 2. Facies summary table.             | 18 |

## ACKNOWLEDGMENTS

This study was sponsored by Nadel and Gussman, Permian in association with the Baylor University Applied Petroleum Studies Program. Project completion was facilitated in part using software donated by IHS Petra<sup>®</sup>. Special thanks are extended to Scott Germann and Michael Matteucci of Nadel and Gussman for their technical assistance and mentorship over the duration of the project and to Joan Gawloski for facilitating our core description at Midland College.

I would like to thank my advisor, Dr. Stacy Atchley, for not only taking such an active interest in my academic development but also for preparing me to “add value” throughout my career. I also express my gratitude to my colleague Brian Crass who has proven to be an able mentor, reliable guide to all things Texan, and more importantly, a friend.

A special thank you is extended to my wife Sasha who has been a never-ending source of support and encouragement throughout my academic career. Thanks for understanding and sharing me with my other love.

## CHAPTER ONE

### Introduction

The Cline Shale, or simply “Cline”, is an unconventional shale play of Pennsylvanian age within the Midland Basin of west Texas. The Midland Basin is a subordinate basin of the greater Permian Basin. The Permian Basin is a 115,000 square mile asymmetrical structural depression located in west Texas and southeast New Mexico (Galley, 1958) that was periodically inundated as part of a Late Pennsylvanian seaway that extended from the Williston Basin of North Dakota to the Appalachian-Ouchita-Marathon orogen of the eastern and southwestern USA (Algeo and Heckel, 2008) (Figure 1). The Permian Basin occupied the former site of the early Paleozoic Tobosa Basin, a shallow basin along the Late Cambrian through Mississippian passive continental margin of North America. The Tobosa Basin was partitioned into numerous subordinate basins as a result of foreland deformation and associated inversion of extensional fault blocks during the Late Paleozoic convergence of Laurasia and Gondwanaland as Pangea was assembled (Tai, 2001; Cawood and Buchan, 2007; Stampfli et al., 2013) (Figure 2). The inverted fault blocks became the locus of Late Paleozoic shallow-marine carbonate and clastic deposition, whereas the adjacent basins were the sites of deeper-water carbonate and clastic deposition (Hills, 1972). The Permian Basin was ultimately subdivided into the Midland and Delaware basins that were separated by the Central Basin Platform (Yang and Dorobek, 1995; Cortez III, 2012).

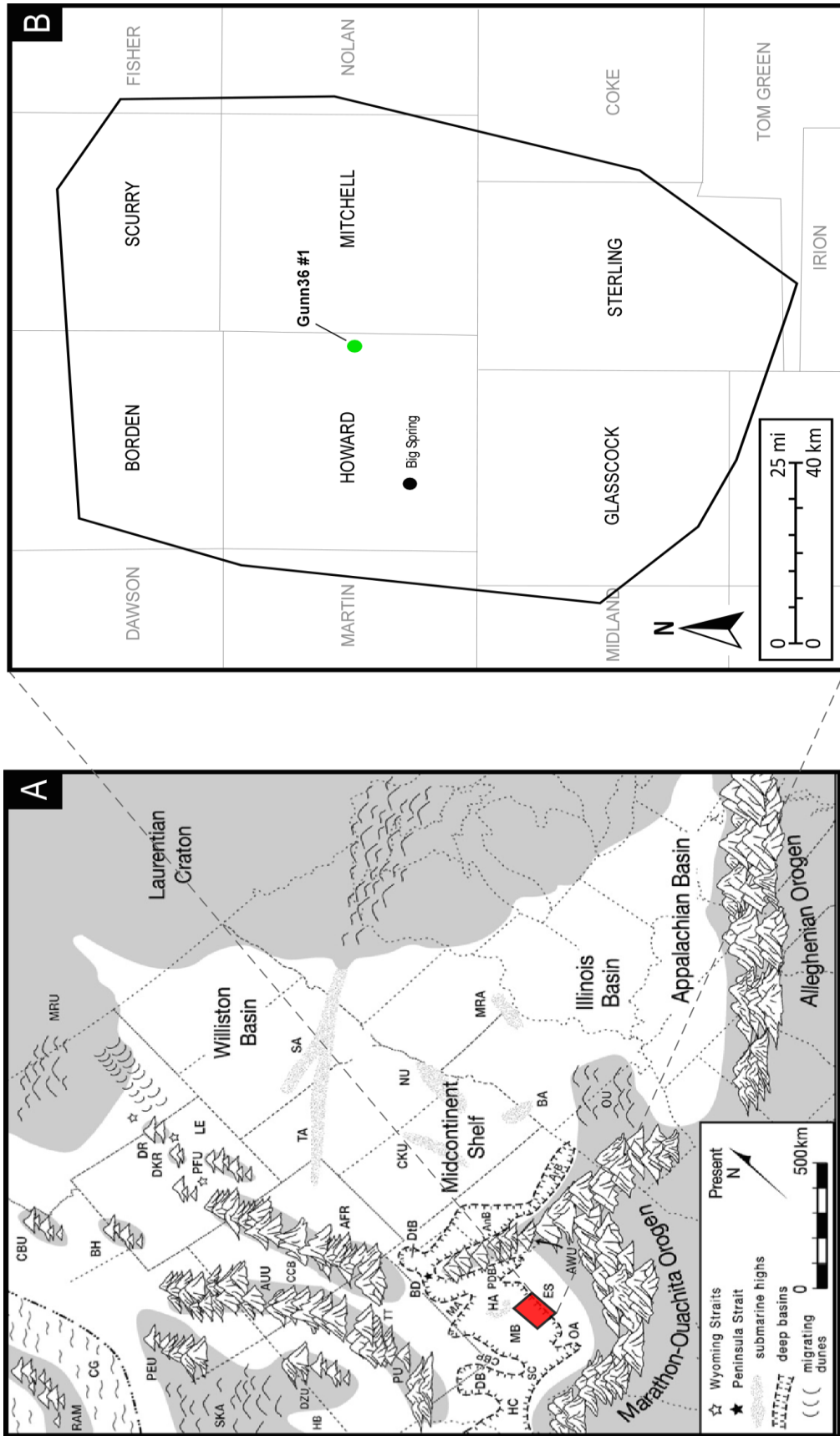


Figure 1. (A) Paleogeography of the Late Pennsylvanian Midcontinent Sea (LPMS) of North America. The location of the study area is indicated by the red rectangle. Abbreviations: CBP = Central Basin Platform, DB = Delaware Basin, ES = Eastern Shelf, HA = Horseshoe Atoll, HC = Hovey Channel, MB = Midland Basin, MA = Matador Arch, OA = Ozona Arch, PDB = Palo Duro Basin, SC = Sheffield Channel (modified from Algeo and Heckel, 2008). (B) Location of the study area. Polygon indicates the boundary of the contours generated using IHS Petra™. County boundaries are provided and counties are labelled by name.

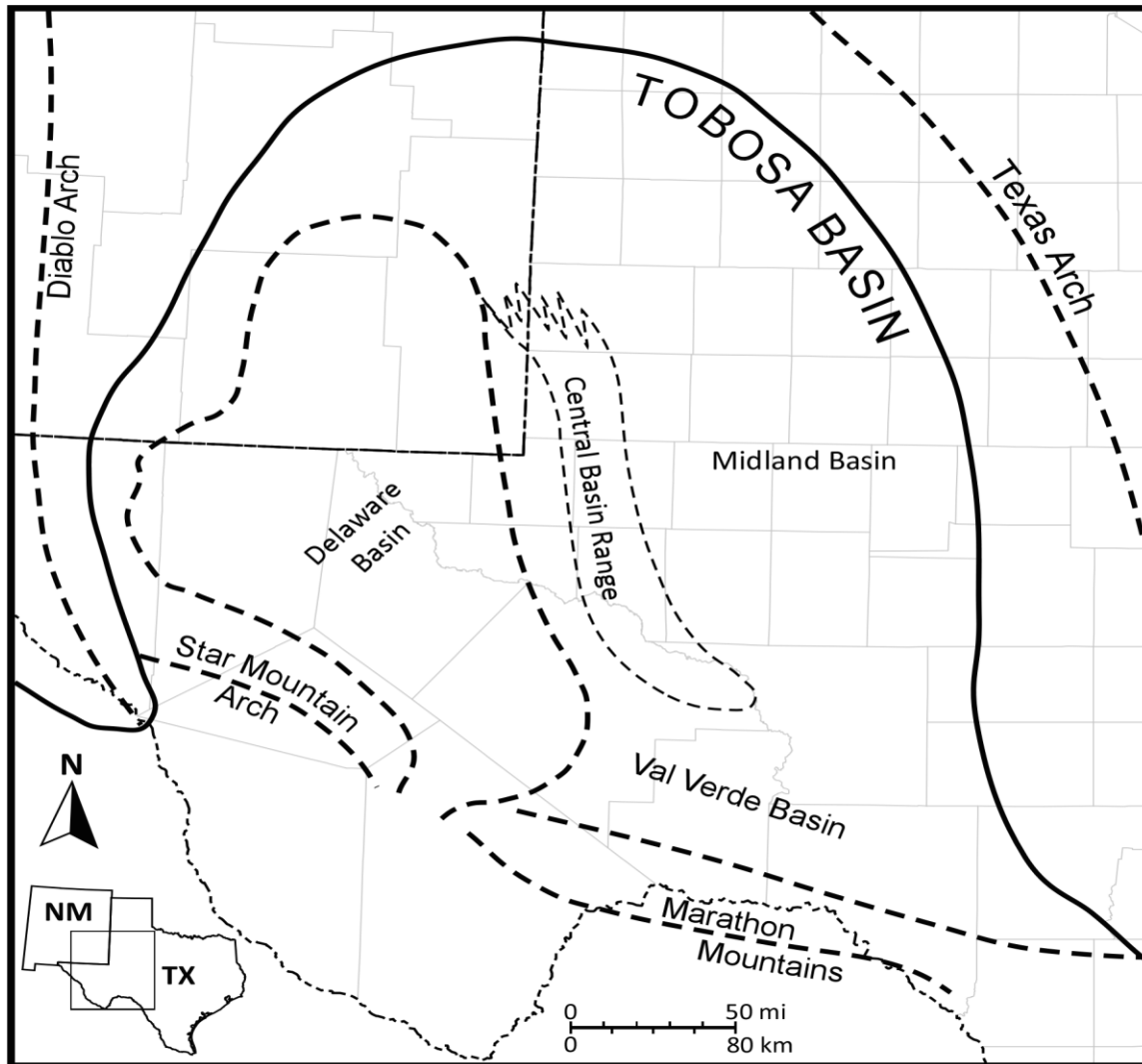


Figure 2. The Early Ordovician extent of the ancestral Tobosa Basin and its subsequent Mississippian subdivisions: Midland Basin, Delaware Basin, Central Basin Platform. Modified from Adams (1965).

The Permian Basin is one of the most mature and prolific onshore oil and gas provinces in the continental United States, with the first economic oil discovery made in 1920 in Mitchell County, Texas (Galley, 1958). Exploration and production in the Permian Basin has continued for more than 90 years, and as of 2005, has yielded cumulative conventional oil production of 30.4 billion barrels primarily from Permian marine carbonate reservoirs (Dutton et al., 2005). The second most productive reservoir interval is Pennsylvanian age marine carbonate and/or sandstone reservoirs (Dutton et al., 2005). Most recently, horizontal drilling coupled with hydraulic fracture stimulation has allowed oil to be produced from low-matrix-permeability unconventional shale reservoirs, e.g. the Barnett Shale (Pollastro et al., 2007; Kinley et al., 2008), Woodford Shale (Cardott and Lambert, 1985; Miceli Romero and Philp, 2012), and Marcellus Shale (Wang and Carr, 2013; Kohl et al., 2014). The Pennsylvanian Cline Shale is a similar unconventional reservoir located within the Midland Basin.

This study evaluates the depositional, stratigraphic and petrologic controls on Cline Shale reservoir quality, and the spatial distribution of core-calibrated petrophysical facies across the area of study within the Midland Basin. The study area is located principally in Borden, Scurry, Howard, Mitchell, Glasscock, and Sterling counties of west Texas (Figure 1).

## CHAPTER TWO

### Paleogeography and Regional Stratigraphy

#### *Midland Basin*

The Central Basin Platform (Figure 3) defines the western boundary of the Midland Basin and formed as a fault bounded, basement-cored uplift that was reactivated and inverted during the Marathon-Ouachita orogeny (Tai, 2001). The neighboring Midland Basin is asymmetrical, with its deepest portion adjacent to the Central Basin Platform (Yang and Dorobek, 1995). During the Pennsylvanian, the western portion of the Midland Basin was characterized by the highest rates of subsidence and associated deepest marine, sediment-starved environments (Adams et al., 1951).

The southern boundary of the Midland Basin includes the Marathon-Ouachita fold and thrust belt and a basement-involved foreland feature similar to the Central Basin Platform that is known as the Ozona Arch (Yang and Dorobek, 1995). The Northwestern, Northern, and Eastern shelves define the northern and eastern limits of the Midland Basin (Walker et al., 1995) (Figure 3).

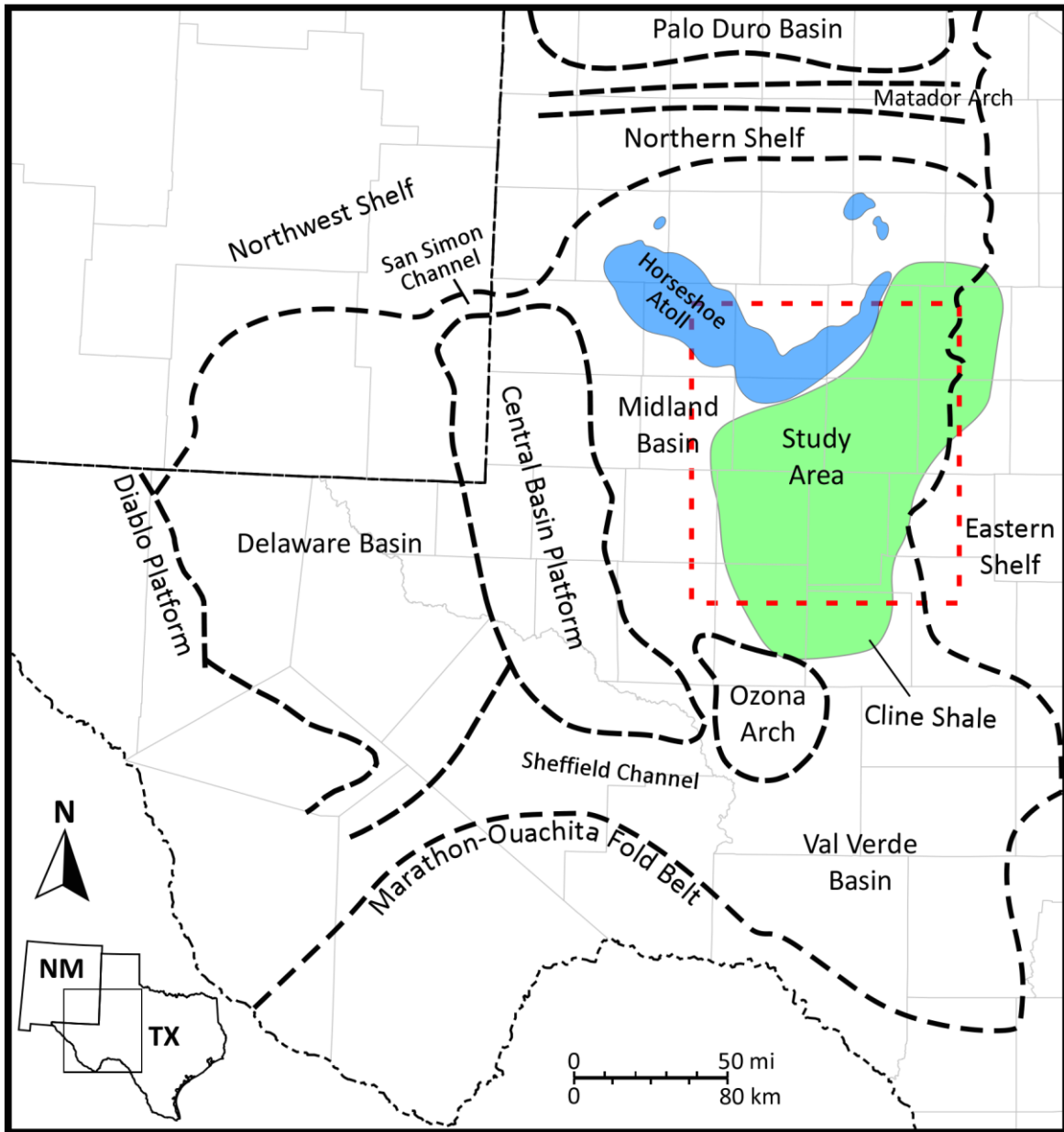


Figure 3. Pennsylvanian paleogeographic and major structural features map of west Texas and southeastern New Mexico (modified from Dutton et al., 2005, and Wright, 2011b). The distribution of the Cline Shale is highlighted in green and was modified from Martin (2012). The study area is indicated by the red dashed rectangle. The position of the Horseshoe Atoll is after Vest, Jr. (1970).

The Horseshoe Atoll is a shallow marine phylloid algal bank complex that occurs within the north-central portion of the Midland Basin and is characterized by a regional crescent-shaped trend (Heck et al., 1952; Vest Jr., 1970; Schatzinger, 1987). Deposition of the atoll began in the early Desmoinesian with aggradational growth that transitioned into retrogradational (backstepping) growth in the mid-late Desmoinesian. The isolated, generally retrogradational nature of the Horseshoe Atoll is due to shallow-marine carbonate nucleation across a basin floor, paleotopographic high within the rapidly subsiding central portion of the Midland Basin. Because the rise in relative sea-level outpaced carbonate sediment production, the Horseshoe Atoll stratal succession records long-period transgression, i.e., retrogradational stratal stacking (Mazzullo and Mazzullo, 1983; Waite, 1993).

#### *Eastern Shelf*

The Ouachita fold and thrust belt, located to the east of the study area, may be the landward source of clastic sediment observed within the Cline Shale. Clastic sediment derived from the Ouachita orogen was transported across the Eastern Shelf and into the Midland Basin (Yang and Kominz, 2003).

#### *Lithostratigraphy*

The Canyon and Cisco groups (Figure 4) were originally described by Cummins, 1891, as cited by Boardman II and Malinky (1985).

The Canyon Group is composed of relatively thin, cyclic alternations between carbonate and lesser amounts of shale (Galloway and Brown Jr, 1973; Schatzinger, 1987).

The Cisco Group is dominated by shale and has an estimated shelf to basin depositional relief of 457 m (1500 ft.) and has an early Permian erosional unconformity as its upper boundary (Saller et al., 1994). These groups have been extensively studied and subdivided on the Eastern Shelf (Boardman II and Malinky, 1985; Yancey, 1986; Ross and Ross, 1988; Boardman II and Heckel, 1989) and their upper Pennsylvanian strata consist primarily of carbonate platform facies that transition basinward into siliclastic and progressively finer-grained, deep-water facies (Yang and Kominz, 2003; Yang and Dorobek, 2012). Basinal facies of the Canyon and Cisco groups have not been studied as thoroughly due to both the lack of outcrop and the prevalence of informal subsurface names that confuse stratigraphic delineation within the basin. One such informal designation is the “Cline Shale”, a term that is used within the Midland Basin to describe the organic-rich shale intervals of the upper Pennsylvanian Canyon and Cisco groups. In this study the “Cline Shale” refers to the organic-rich shale interval between the Pennsylvanian Strawn and Cisco groups (Figure 4).

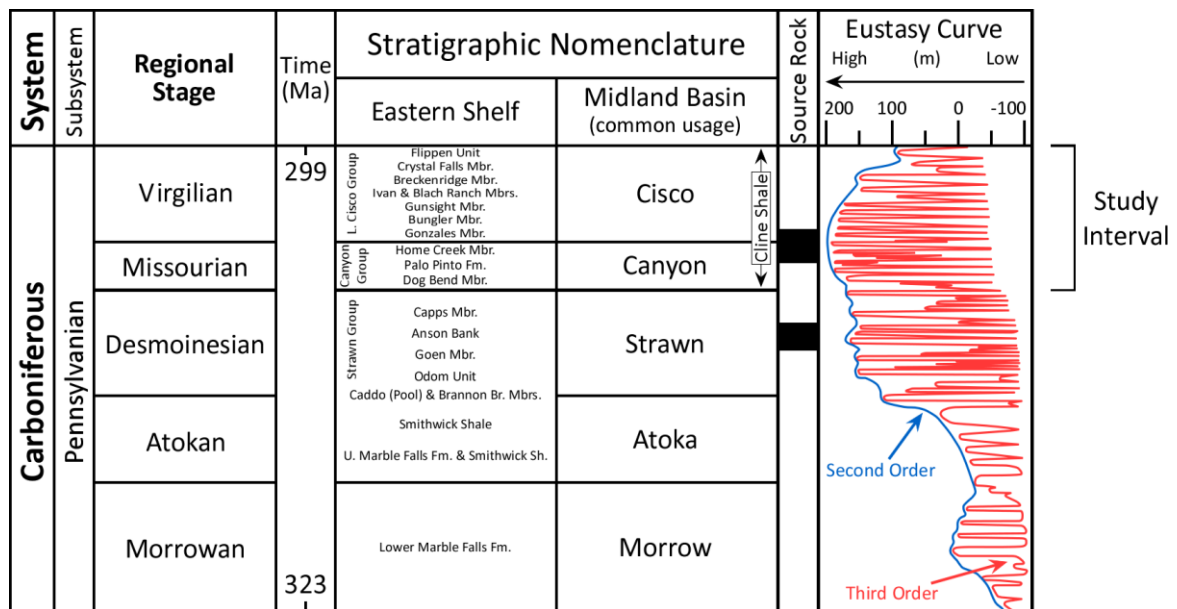


Figure 4. Stratigraphic correlation chart for Carboniferous (Pennsylvanian) strata within the Midland Basin and Eastern Shelf of west Texas (modified from Wright, 2011b). The highlighted source rock intervals are from Sarg et al. (1999). The eustatic sea level curve is from Ross and Ross (1987). The apogee of long period sea level rise corresponds with Cline Shale “source rock” deposition. The long period rise in sea level during the Strawn and Cisco coincide with the initial aggradational and subsequent retrogradational stacking of strata within the Horseshoe Atoll.

## CHAPTER THREE

### Methods

#### *Stratigraphic Correlation*

A detailed stratigraphic framework was constructed across the study area by correlating 138 well logs within a grid of 6 stratigraphic cross sections (Figure 5). The Upper Strawn Formation top was selected as a stratigraphic datum owing to its deposition as an extensive, uniformly thick unit across the study area (Wright, 2011a). The Upper Strawn is composed primarily of bedded limestone and thinly bedded shale, and is characterized by a pronounced drop in natural gamma radiation (Figure 6). Within the study interval two additional formation tops were identified on well-logs: 1) the “Three Fingers” is a marker bed recognized by a triplet set of repeated thinly bedded shales that are thought to represent the boundary between the Canyon and Cisco groups, and 2) the top of the Cline Shale is a doublet marker of thinly bedded shales located at the upper limit of the study interval (Figure 6).

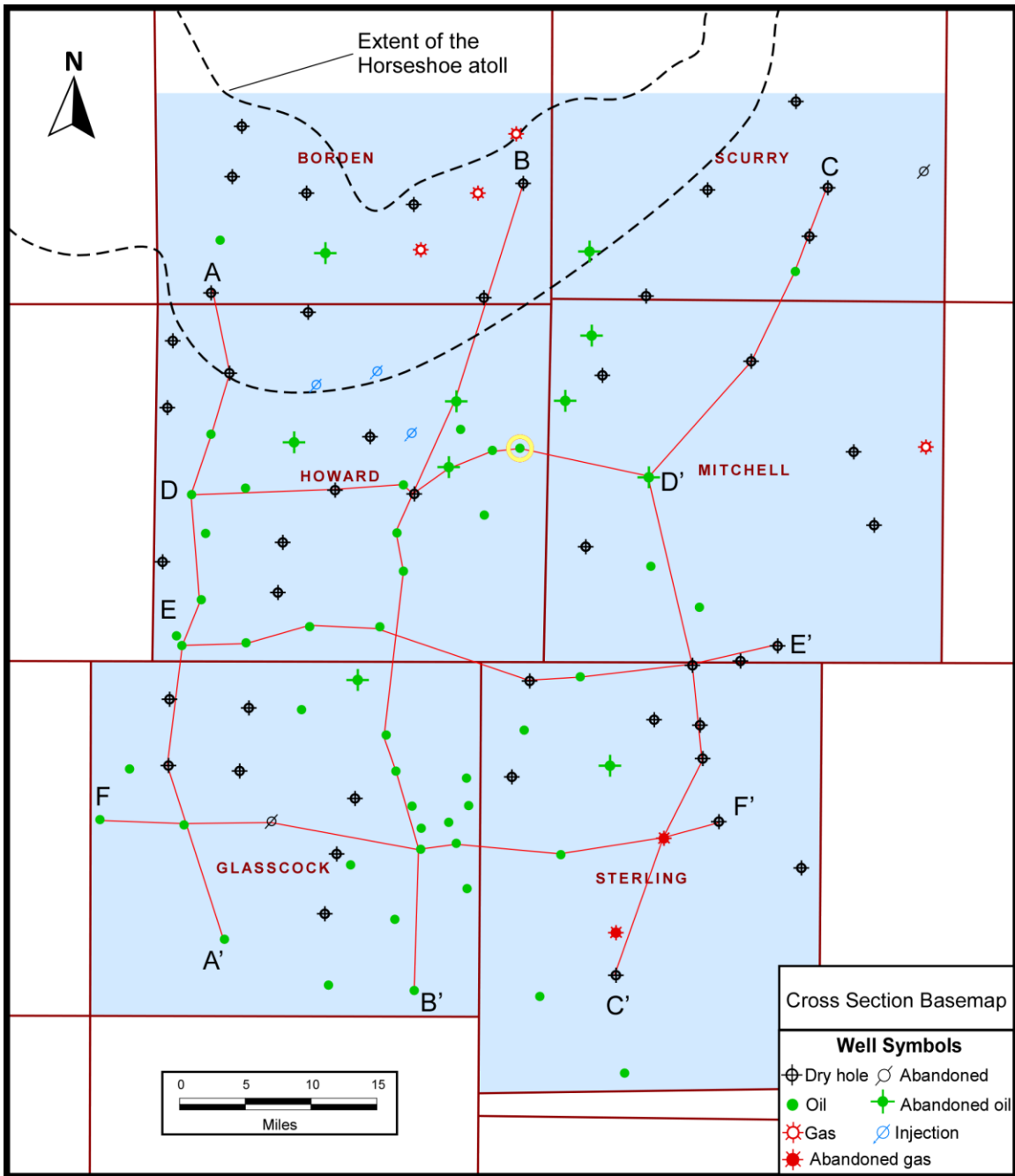


Figure 5. Basemap of study area with cross-section grid highlighted. The location of the Gunn36 #1 cored well is highlighted with a yellow circle. Data used in the stratigraphic correlation include logs from 138 wells within a grid of 6 cross-sections. Note that only 111 wells are displayed to prevent data overposting in areas of concentrated drilling activity. The position of the Horseshoe Atoll is modified from Vest Jr. (1970).

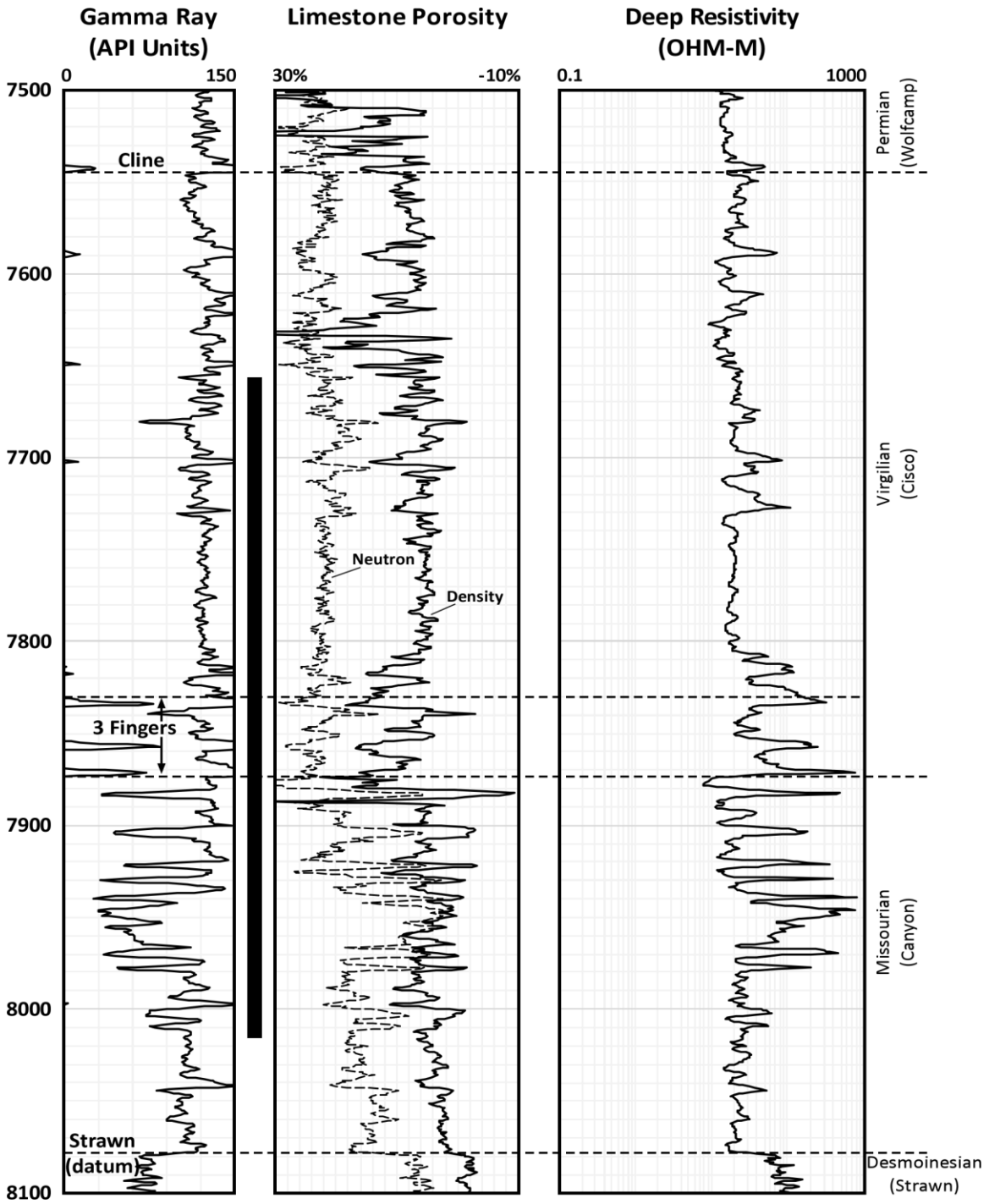


Figure 6. Type log of the study interval (Gunn36 #1 well). Stratigraphic tops include the Strawn, the Three Fingers base and top (the top of which also approximates the boundary between the Canyon and Cisco Groups), and the Cline top. The black bar indicates the cored interval (see description in Appendix D). Modified from Crass (2015).

### *Core Description*

The entire 111 m (365 ft.) of core available for the Gunn36 #1 well was described in detail at Midland College, Midland, Texas (Appendix D). Core descriptions were completed at a resolution of 15 cm (0.5 ft.) and include documentation of the vertical distribution of lithology, carbonate textural classification according to Dunham (1962) as modified by Embry and Klovan (1971), grain type, grain size, sedimentary structures, facies, ichnofabric index (Droser and Bottjer, 1986; Bottjer and Droser, 1991), color, fracture density, cement type and occurrence, and effervescence with dilute hydrochloric acid (Appendix D).

### *Facies Predictions*

The Gunn36 #1 core description was digitized and depth-shifted to coincide with digital petrophysical well log data. Core depositional facies were compared against various well log data to determine whether facies can be predicted in wells that lack core control (Crass, 2015). Cross plots of gamma ray versus density porosity suggest that a numerical transform using bracketed parameter range cutoffs allows for facies prediction (Crass, 2015) (Table 1). Wells having only raster images of gamma ray and density porosity were digitized in the main module of IHS Petra™ before the model was applied to all wells. The transform was then applied using IHS Petra™ software and the resulting petrophysical facies were plotted in the depth track for wells viewed in the Cross Section Module of IHS Petra™.

Table 1. Guidelines for facies prediction from open-hole well logs.

Model Derived Petrofacies	Depositional Facies Equivalent	Parameters for Well Log Prediction
Dolomitized Carbonate Beds (DCB)	Primarily LCF and SBM. Lesser IGC and MBM.	GR = 0 to 150 API DPHI = -10% to -2%
Carbonate Gravity Flows (CGF)	Primarily LCF and GSC. Lesser MBM.	GR = 0 to 60 API DPHI = -2% to 30%
Mixed Carbonate and Mud (MCM)	Primarily MBM, SBM and LCF. Lesser GSC, LCM and MSC.	GR = 60 to 105 API DPHI = -2% to 30%
Non-Reservoir Shale (NRS)	Primarily MBM and SBM. Lesser BLM.	GR 105 to 300 API DPHI = -10% to 10%
Organic Rich Shale (ORS)	Primarily BLM. Lesser MBM and SBM.	GR = 105 to 300 API DPHI = 10% to 30%
Shallow Marine Carbonate (SMC)	N/A	GR 0 to 30 API DPHI = -2% to 30%
Wash-Out Zone (WOZ)	N/A	GR not used DPHI = above 30%

### *Structure Maps*

Structure contour maps were prepared from the tops of the three main study units correlated across the grid of well log cross sections (138 total wells), i.e., the Strawn, Three Fingers, and Cline. Stratigraphic surface “picks” were placed using the Cross Section Module of IHS Petra™ and maps were subsequently generated using the Mapping Module. The resulting contour maps were then exported as ESRI shape files that were then accessed in the ESRI ArcGIS™ ArcMap™ module where they were subsequently exported in EPS format. The EPS files were then imported into ACD Canvas™ where final versions of all maps were hand-edited and refined to publication quality.

### *Facies Maps*

Contour maps of cumulative facies thickness and distribution were generated for each of the petrophysical facies in a manner similar to the structure contour maps. An additional isopach map of the Cline interval, i.e., the strata between the Strawn and Cline stratigraphic tops, was also prepared.

## CHAPTER FOUR

### Observed Facies and Environments

#### *Introduction*

To date, the Cline Shale has generally not been studied academically. The Cline Shale has been described by the Midland Basin oil industry as the stratigraphic interval that includes the basinal equivalents of the predominantly shelfal Canyon and Cisco groups, and has generally been interpreted as a thin, dark shale that accumulated within a rapidly subsiding and sediment starved basin (Adams et al., 1951; Adams, 1962).

Whereas the Canyon and Cisco are well-defined on the Eastern Shelf, their occurrence in the Midland Basin is not, inasmuch as the Cline Shale transitions from relatively thick Canyon and Cisco shelf carbonates, updip, to thin, condensed basinal shales, downdip (Mazzullo and Reid, 1989). Sediment gravity flows that contain both skeletal grains and lithoclasts are increasingly abundant from basinal positions towards the Horseshoe Atoll, and are typically more common in Canyon equivalent strata (Hobson et al., 1985a; Mazzullo and Reid, 1989; Cortez III, 2012).

Eight depositional facies (Table 2) are distinguished within the study area on the basis of grain type, grain size, sedimentary structures, and ichnofabric index, i.e., a numerical scale from 1-5 such that 1 represents no bioturbation and complete preservation of mechanical sedimentary structures, and 5 represents complete bioturbation and total destruction of mechanical sedimentary structures (Bottjer and Droser, 1991).

Table 2. Observed facies summary table of the diagnostic criteria by which depositional facies were identified in the Gunn36 #1 core

Name	Black Laminated Mudrock	Mottled Black Mudrock	Skeletal Black Mudrock	Laminated Carbonate Mudstone	Mud-Supported Carbonate	Grain-Supported Carbonate	Lithoclastic Carbonate Floatstone	Inversely Graded Carbonate
Environment	offshore	offshore	offshore	offshore to toe of slope	toe of slope	middle slope	middle to upper slope	upper slope
Inferred Processes	pelagic to hemipelagic sediments	biologically reworked hemipelagic sediments	platform-swept skeletal in hemipelagic sediments	turbidity flow: Bouma D-E	turbidity flow: Bouma C-D	turbidity flow: Bouma A	debris flow	grain flow
Typical Siliclastic Mud Content	>90%	>60%	60%-90%	<10%	<10%	<10%	30%-70%	<10%
Average Grain Size	silt and clay	silt and clay	mud and pebbles	lower silt and clay	upper silt to fine sand	medium to very-coarse sand	mud and pebbles	medium sand to pebble
Ichnofabric Index	1-2	3-5	2-5	1-2	1	1	1	1
Physical Sedimentary Structures	mm lamina	discontinuous mm lamina	mm lamina	mm lamina	mm lamina, current ripples	normal grading	none	inverse grading
Representative Core Photo	Figure 7A	Figure 7B	Figure 7C	Figure 7D	Figure 7E	Figure 7F	Figure 7G	Figure 7H
Facies Code	<b>BLM</b>	MBM	SBM	LCM	MSC	GSC	LCF	IGC

### *Black Laminated Mudrock – BLM*

*Description:* BLM is a black to dark gray siliciclastic mudrock composed of mm-laminated silt and clay sized siliciclastic sediment (90%) with interspersed lamina of gray calcareous silt (10%) (Figure 7A). Phosphate nodules are common in the darkest colored sections and have an average diameter of 4 cm. Skeletal fragments are rare when present and are typically brachiopod/bivalve fragments. This facies has little to no bioturbation and is assigned an ichnofabric index of 1-2.

*Interpretation:* The lack of oxidation and bioturbation along with high mud content suggest deposition in a low-energy offshore, oxygen-restricted setting that corresponds to periods of maximum transgression (Heckel, 1977; Boardman II and Malinky, 1985; Yancey, 1986).

### *Mottled Black Mudrock – MBM*

*Description:* MBM is a dark to light gray mudrock with silt to clay sized siliciclastic sediment (Figure 7B). Sedimentary structures include mm-scale laminae that are discontinuous and wavy to convolute. The rock fabric is assigned an ichnofabric index of 3-5. Carbonate allochems are uncommon (<10%) but can include fusulinids, crinoids, and brachiopod/bivalve fragments. Carbonate mud composition may be as high as 40%. This facies commonly overlies either the carbonate LCM, MSC, and GSC facies, or the siliciclastic BLM facies.

*Interpretation:* The reduction in siliciclastic mud content coupled with the increase in bioturbation and calcareous sediments suggest deposition in an offshore, normal marine environment that is more oxygenated than that of the BLM facies (Heckel, 1977; Boardman II and Malinky, 1985; Hobson et al., 1985a; Yancey, 1986).

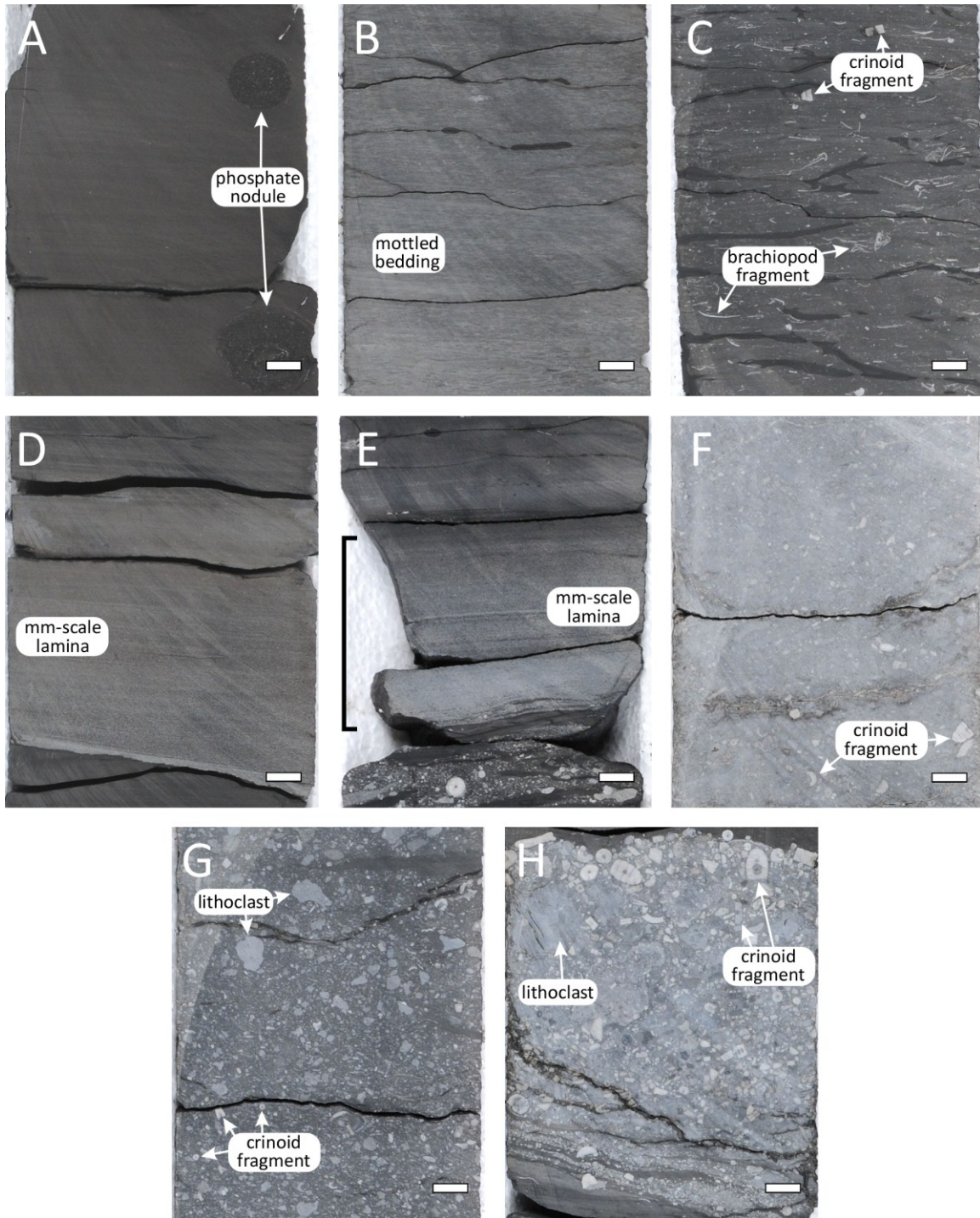


Figure 7. Representative core photographs of depositional facies observed in the Gunn36 #1 well. Scale bar is 1cm. (A) Black laminated mudrock facies at 7893ft. (B) Mottled black mudrock facies at 8024 ft. (C) Skeletal black mudrock facies at 7918.5 ft. (D) Laminated carbonate mudstone facies at 7942 ft. (E) Mud supported carbonate facies at 7955 ft. (F) Grain supported carbonate facies at 7969 ft. (G) Lithoclastic carbonate floatstone facies at 7994.5 ft. (H) Inversely graded carbonate facies at 8032.5 ft.

### *Skeletal Black Mudrock – SBM*

*Description:* SBM is a dark to light gray mudrock with 60-90% mud to clay sized siliciclastic sediments (Figure 7C). The remaining 10-40 percent of the sediment volume is dominated by carbonate mud and lesser allochems of brachiopods, crinoids and fusulinids. The bioturbation index ranges from moderate to high (2-5) with mm-lamination preserved when unobscured by bioturbation. This facies most commonly overlies the MBM or BLM facies.

*Interpretation:* The high siliciclastic mud content, variable bioturbation and abundance of brachiopod fragments suggests deposition in an oxygenated, basinal environment that is relatively more proximal to a shallow-marine carbonate shelf or bank (Bottjer and Droser, 1991; Hickey and Henk, 2007).

### *Laminated Carbonate Mudstone – LCM*

*Description:* LCM is a light gray carbonate mudstone that is dominated by mm-scale lamina with <10% siliciclastic mud (Figure 7D). This facies is typically thin to medium bedded (76 mm average thickness but up to 152 mm). The LCM commonly sharply overlies the LCF and MCM facies and grades upward into the LCF, SBM or BLM facies. Bioturbation is rare, and the rock fabric is classified as having an ichnofabric index of 1-2. Skeletal fragments are also rare.

*Interpretation:* The abundance of laminated carbonate mud, sharp lower contacts with the SBM and LCF facies and gradational upper contacts with the SBM, BLM and LCF facies suggest deposition of allochthonous sediments by turbidity currents on the basin floor and/or toe of slope. Associated deposits are classified as the T<sub>d</sub> and T<sub>e</sub>

divisions of the ideal Bouma succession (Bouma, 1962; Enos and Moore, 1983; Shanmugam, 1997).

#### *Mud Supported Carbonate – MSC*

*Description:* MSC is a medium to light gray wackestone with abundant mm-lamina and current ripples (Figure 7E). This facies is characterized by normal grading and a bimodal grain size distribution of mud-supported fine sand. The MSC is medium bedded (average bed thickness of 190 mm) and commonly both under- and overlies the siliciclastic mud dominated SBM and MBM facies. The basal contact is sharp and wavy, whereas the upper contact is typically gradational. The MSC has an ichnofabric index of 1.

*Interpretation:* The abundance of carbonate mud, mm-lamina and ripples suggest deposition by a current that is stronger than that invoked for the LCM facies. Deposits are classified as the T<sub>c</sub> and T<sub>d</sub> divisions of the ideal Bouma succession, and are interpreted to have accumulated in a lower slope to toe of slope setting (Bouma, 1962; Enos and Moore, 1983; Shanmugam, 1997).

#### *Grain Supported Carbonate – GSC*

*Description:* GSC is a light gray, medium to coarse-grained carbonate packstone (Figure 7F). Carbonate allochems are abundant and include fragments of crinoids, brachiopods, bryozoans, fusulinids and lesser carbonate lithoclasts. Beds are normally graded and average 304 mm in thickness. Lower contacts are wavy and generally overlie the MBM, LCF and SBM facies.

Upper contacts are gradational and commonly transition into the MBM facies and less so the SBM and LCF facies. The GSC is characterized by an ichnofabric index of 1.

*Interpretation:* The abundance of coarse carbonate grains, presence of lithoclasts and absence of mechanical sedimentary structures suggest turbidity deposition in a shelf slope setting. Deposits are classified as the T<sub>a</sub> division of the ideal Bouma succession (Bouma, 1962; Enos and Moore, 1983; Shanmugam, 1997).

#### *Lithoclastic Carbonate Floatstone – LCF*

*Description:* LCF is a grey carbonate floatstone with abundant coarse lithoclasts and lesser skeletal fragments of crinoids, brachiopods and fusulinids (Figure 7G). The facies is ungraded, poorly-sorted and chaotic, and is characterized by a bimodal grain size distribution of matrix-supported medium sand to pebble-sized clasts. Lower bed contacts are sharp, wavy or inclined. At the lower contact grains are, in some cases, observed penetrating the underlying BLM, MBM or SBM facies.

Upper contacts are sharp or gradational and inclined, and commonly overlie the siliciclastic mudstone facies or the LCM and IGC carbonate facies. Bioturbation is absent.

*Interpretation:* The unsorted, chaotic fabric, sharp (erosional) lower contact, and abundance of coarse lithoclasts suggests debris-flow deposition in the middle to upper shelf slope (Enos and Moore, 1983; Shanmugam, 1997).

#### *Inversely Graded Carbonate – IGC*

*Description:* IGC is a light gray carbonate packstone to grainstone (Figure 7H). Deposits are inversely graded and consist of grain supported medium sand to pebble-

sized lithoclasts, and fragments of crinoids, brachiopods, bryozoans and fusulinids. Lower contacts are inclined and irregular and may have grains that penetrate into the underlying MBM or LCF facies. Upper contacts are sharp and irregular and usually underlie the MBM or LCF facies. Bioturbation is absent.

*Interpretation:* The inverse grading and abundance of grains suggests upper slope deposition by grain flows proximal to the source of carbonate allochems (Enos and Moore, 1983).

#### *Petrophysical Facies Description*

Five log-based petrofacies were identified through the application of statistical transforms developed by Crass (2015).

Table 1 and Figure 8 summarize the diagnostic petrophysical criteria by which each of these core-based petrofacies are defined and lists their constituent depositional facies. Two additional petrophysical facies were created that were not based on depositional facies observed in core. These facies were created to account for the predicted presence of inferred shallow-marine carbonates, as well as to account for the presence of borehole washouts observed in well logs.

#### *Shallow Marine Carbonate – SMC*

The SMC facies was created to account for shallow-marine carbonates associated with the Horseshoe Atoll, and was modeled after similar shallow-marine platform deposits described by numerous workers (Myers et al., 1957; Mazzullo and Mazzullo, 1983; Hobson et al., 1985b; Schatzinger, 1987; Waite, 1993). The SMC is defined as having a GR range of 0-30 API units and a DPHI range of -2-30 percent (Table 1).

### *Wash-Out Zone – WOZ*

The WOZ facies was created to account for the occurrence of borehole washouts recorded on the wireline logs. Borehole washouts are most common in thin shales and occur when the wellbore wall collapses or caves in response to excessive fluid pressure, borehole stress, or unconsolidated sediments (Doveton, 1994). Borehole washouts are characterized by a caliper log value exceeding the drill bit diameter and DPHI value greater than 30 percent.

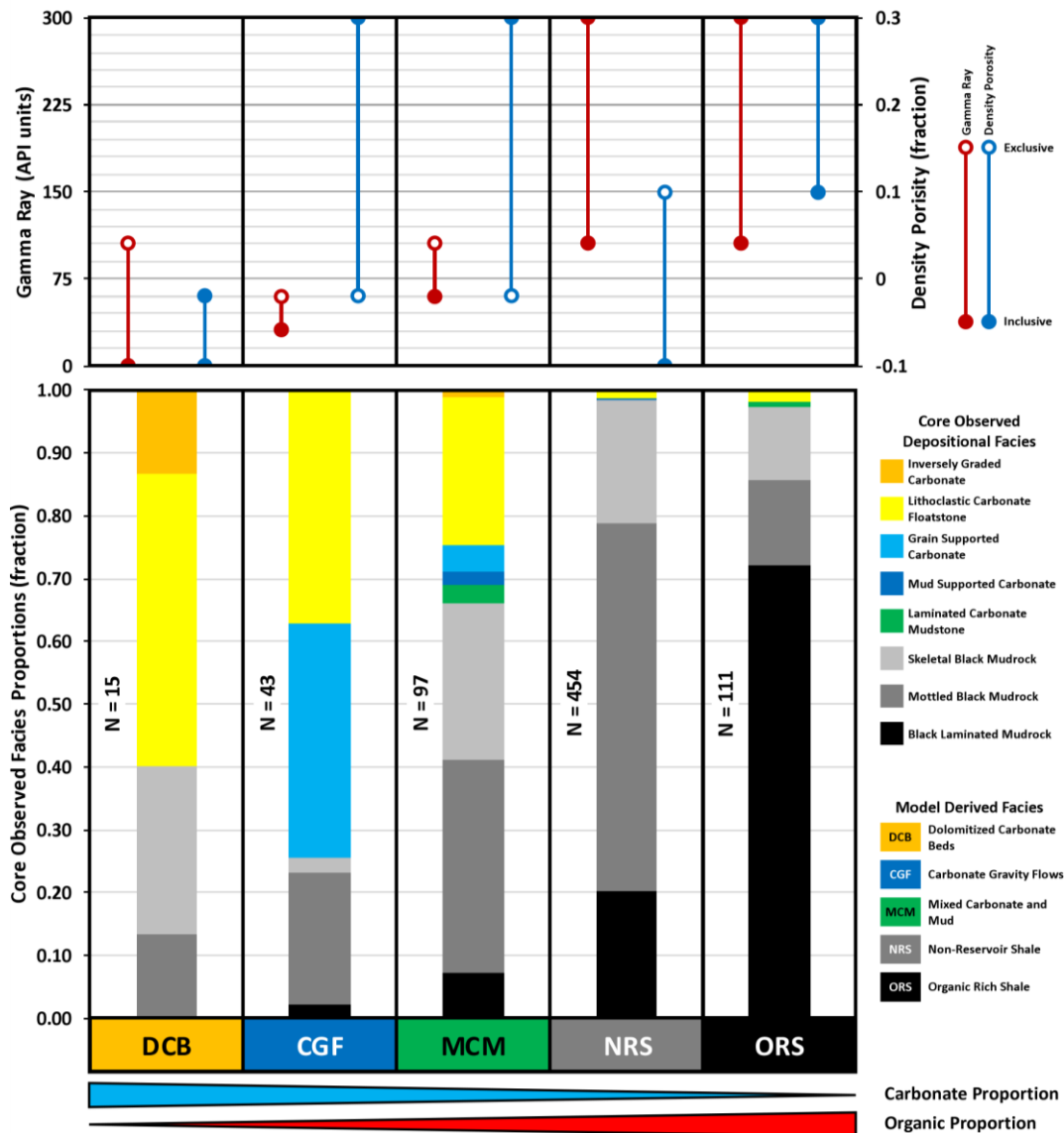


Figure 8. Petrophysical facies from the Gunn36 #1 well and their diagnostic range of gamma ray and density porosity cut-offs, along with the proportion of core observed facies contributions to each petrophysical facies. The relative trends in carbonate to organic content are also indicated at the bottom of the figure. Carbonate proportions are based on the reactions of each facies to dilute hydrochloric acid. Organic proportions were established based on core analyzed TOC (Figure 11). Carbonate and organic content are inversely related and likely reflect both the introduction of oxygen and the dilution of organic matter by carbonate gravity flows. Modified from Crass (2015).

## CHAPTER FIVE

### Distribution of Reservoir Quality

The most prospective petrofacies include the ORS and to a lesser extent the NRS (Crass, 2015). Crass (2015) determined relative reservoir potential by estimating the proportion of total organic carbon (TOC). Both the Passey (Passey et al., 1990) and Schmoker (Schmoker and Hester, 1983) methods were evaluated but the density porosity log-based “Schmoker equation” was preferred because it produced results more similar to those obtained from the laboratory analyses of core plugs that yielded a TOC range of 1-10 wt% (Figure 9). The “Schmoker equation” is as follows:

$$TOC (wt\%) = \left( \frac{156.956}{\rho b} \right) - 58.271, \text{ where:}$$

$\rho b$  = bulk density value from wireline log data

156.956 and 58.271 = empirical constants relating organic matter density, matrix density, and a ratio between weight percents of organic matter and organic carbon with generic shale values as prescribed by Asquith (2012) (Crass, 2015).

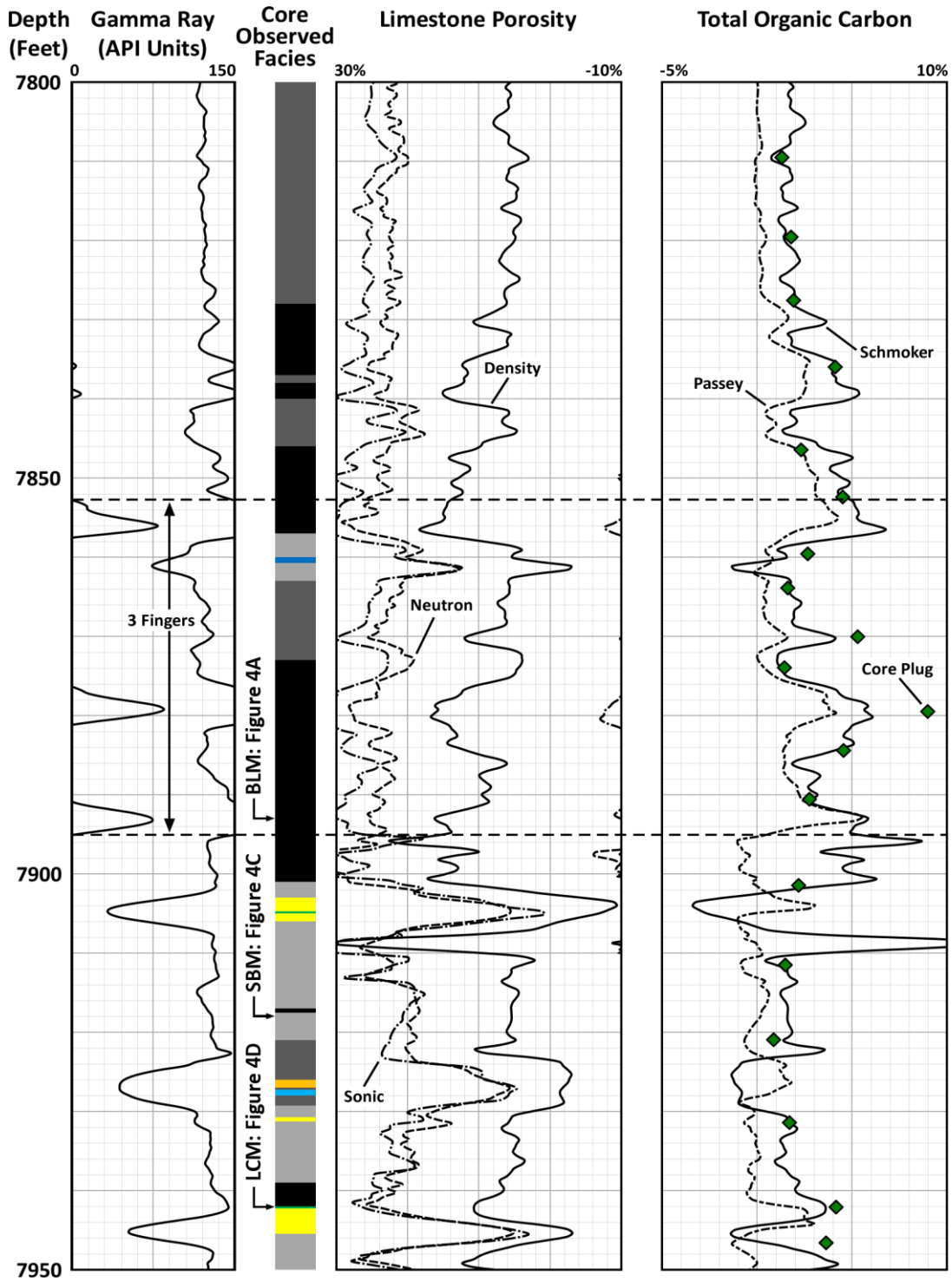


Figure 9. Well logs comparing the Passey and Schmoker methods to laboratory TOC measurements from core plugs. The Schmoker method more closely matches laboratory TOC measurements whereas the Passey method consistently underestimates TOC. See Table 2 for core observed facies color codes and Figure 7 for core photographs of the captioned facies. Modified from Crass (2015).

The relationships between core-derived depositional facies, petrophysical facies and organic richness were evaluated with the use of box and whisker plots that compared facies against Schmoker-calculated TOC estimates. Higher TOC values correspond with the deep-water, siliciclastic-dominated facies (SBM, MBM and BLM) and lower TOC values with the shallow-water, carbonate-dominated facies (IGC, LCF, GSC, MSC, and LCM) (Figure 10).

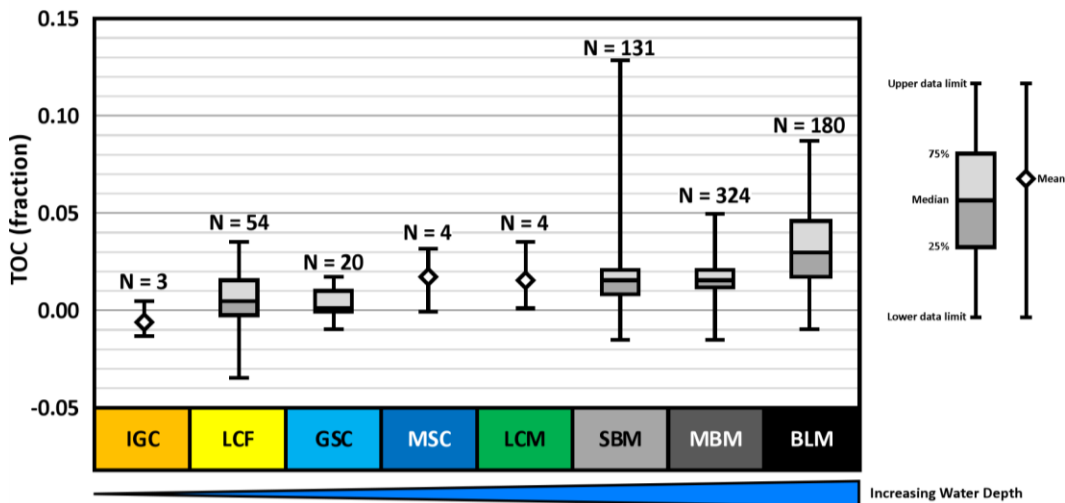


Figure 10. Box and whisker plot of depositional facies versus Schmoker-derived TOC. Deeper water, siliciclastic dominated facies generally correspond with higher TOC values. Refer to Table 2 for facies codes. Modified from Crass (2015).

A corresponding trend exists with the petrophysical facies. The carbonate related facies (DCB, CGF), and the transitional MCM facies have lower TOC values and the siliciclastic-dominated NRS and ORS facies have higher TOC values (Figure 11). The ORS petrofacies has highest TOC values (range from 3-13%, average of 4.5%) and is the most prospective potential reservoir.

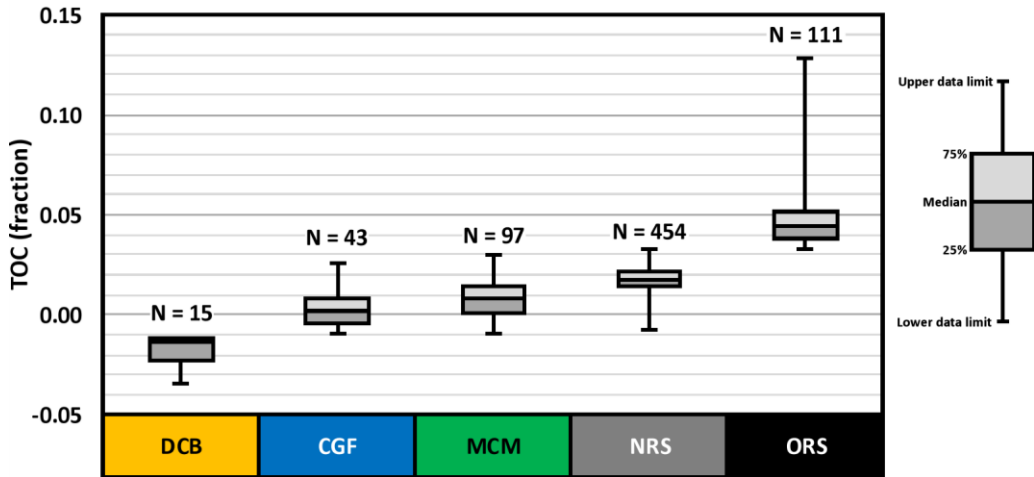


Figure 11. Box and whisker plot of petrophysical facies versus Schmoker-derived TOC. The ORS is most organic rich and has the highest reservoir potential.

Cumulative isopach maps of both the ORS and NRS petrofacies illustrate the influence of the Horseshoe Atoll and Eastern Shelf on both their distribution. Both facies thin towards the atoll and thicken basinward (Figures 12 and 13). The ORS thickens in a basinward direction into southwest Glasscock County and thins to the east towards the Eastern Shelf in Sterling and Mitchell Counties (Figure 12). Noteworthy trends of the NRS include northeastward thinning of the facies from southeast Scurry County in the north to Glasscock County in the south, and thickening towards the Eastern Shelf in southeast Mitchell and Sterling Counties (Figure 13).

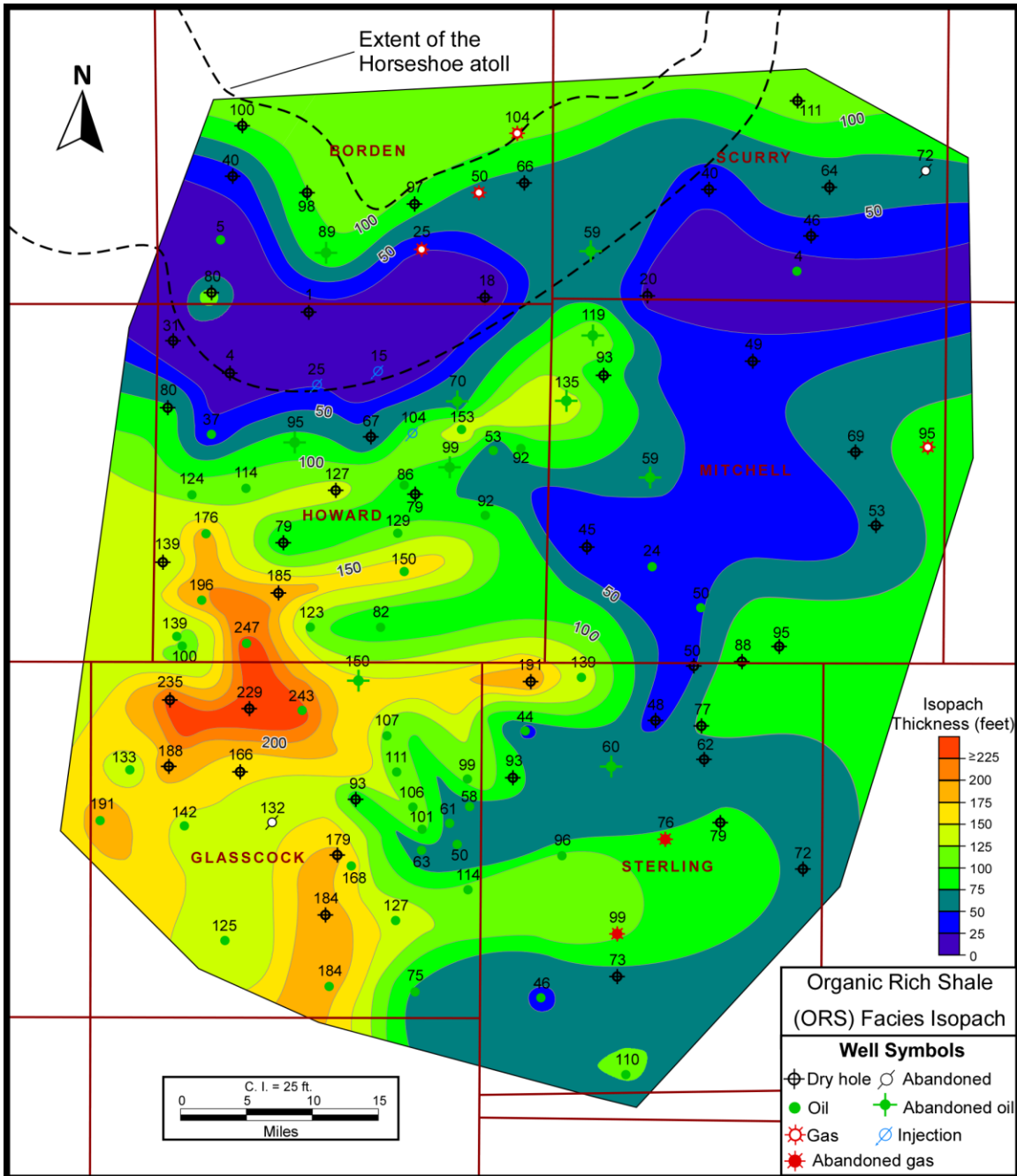


Figure 12. Organic Rich Shale (ORS) facies cumulative isopach map. Facies distribution is strongly influenced by the proximity to the Horseshoe Atoll and Eastern Shelf (which lies just outside of the study area). The outline of the Horseshoe Atoll is depicted by the dashed black polygon in the northern portion of the study area. The position of the Horseshoe Atoll is modified from Vest Jr. (1970).

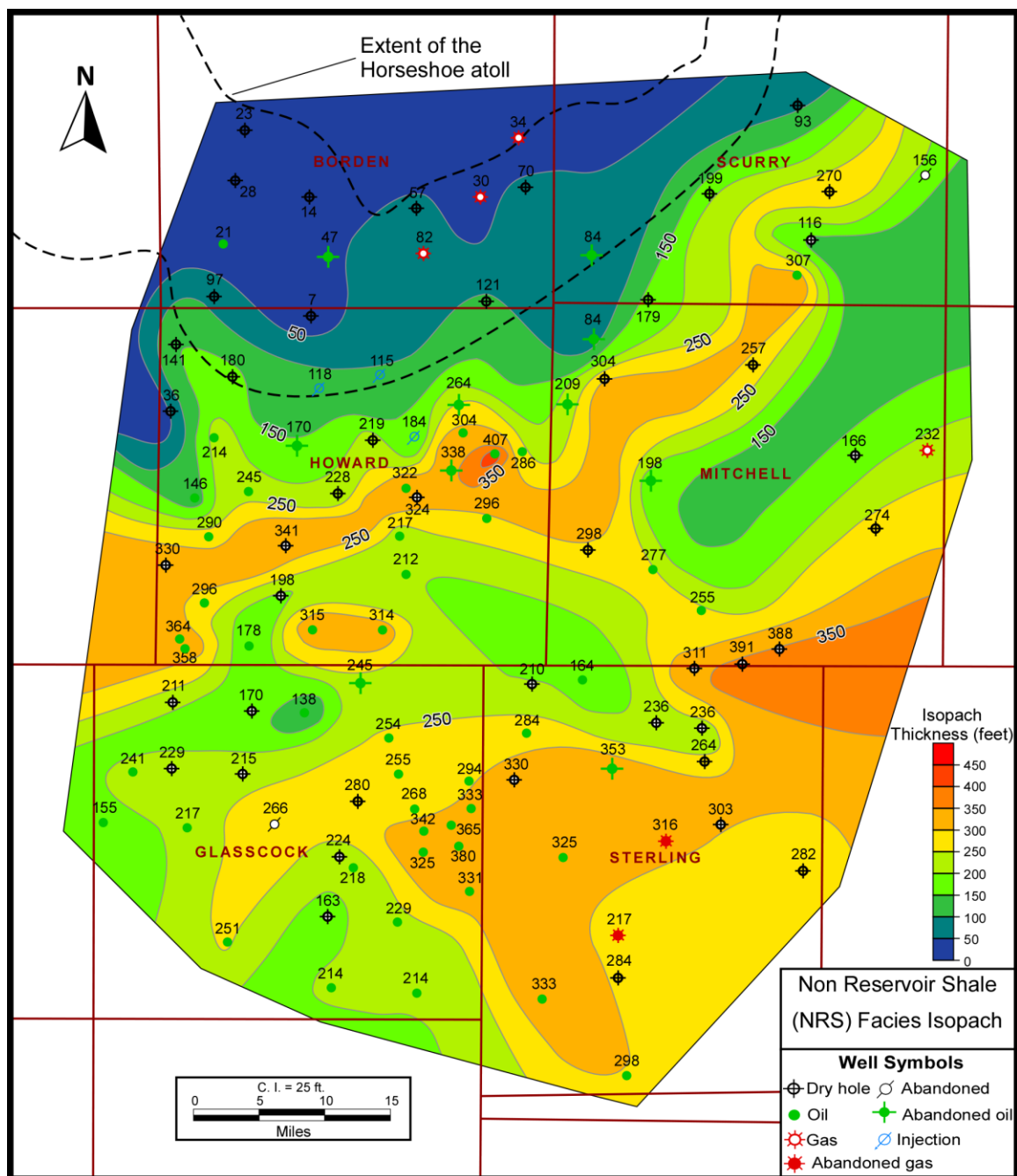


Figure 13. Non-Reservoir Shale (NRS) facies cumulative isopach map. Facies distribution is influenced by the proximity to the Horseshoe Atoll and Eastern Shelf (which lies just outside of the study area). The outline of the Horseshoe Atoll is depicted by the dashed black polygon in the northern portion of the study area. The position of the Horseshoe Atoll is modified from Vest Jr. (1970)

Proximity to the Horseshoe Atoll has a direct influence on the organic richness of the ORS and NRS facies. The Atoll was a major source of carbonate debris that was shed into the basin as gravity or debris flows. Carbonate gravity flows diluted organic matter content as a result of both associated high sedimentation rates (Ibach, 1982; Tyson, 2001; Lash and Blood, 2014) and introduction of oxygen and/or deposit feeding organisms from shallower-water to deeper-water settings (Davis et al., 1989; Mertz Jr, 1989; Landing, 2012). Carbonate gravity flows (represented by the CGF facies) generally decrease in abundance south of the Horseshoe Atoll, with the exception of Scurry County where the facies extends as an elongate trend basinward independent of the atoll (Figure 14). This feature may be related to the debris flows recognized on the edges of the SACROC and Cogdell fields) in Scurry County and may be the result of channels cut into the Horseshoe Atoll while the reef was exposed during sea-level lowstands (Reid and Tomilson-Reid 1991; Walker, 1995). The occurrence of channelized debris flows is more prevalent on the windward (northeastern) extent of the Atoll due to a combination of its increased topographic relief (Burnside, 1959), and northeasterly wave approach from prevailing winds (Walker, 1995). The inverse relationship between these carbonate gravity flows and organic matter abundance is illustrated in the facies ratio map ORS/CGF (Figure 15). In areas near the atoll, and more notably, proximal to the inferred channel where the CGF facies extends basinward, there is a marked reduction in the abundance of the ORS facies.

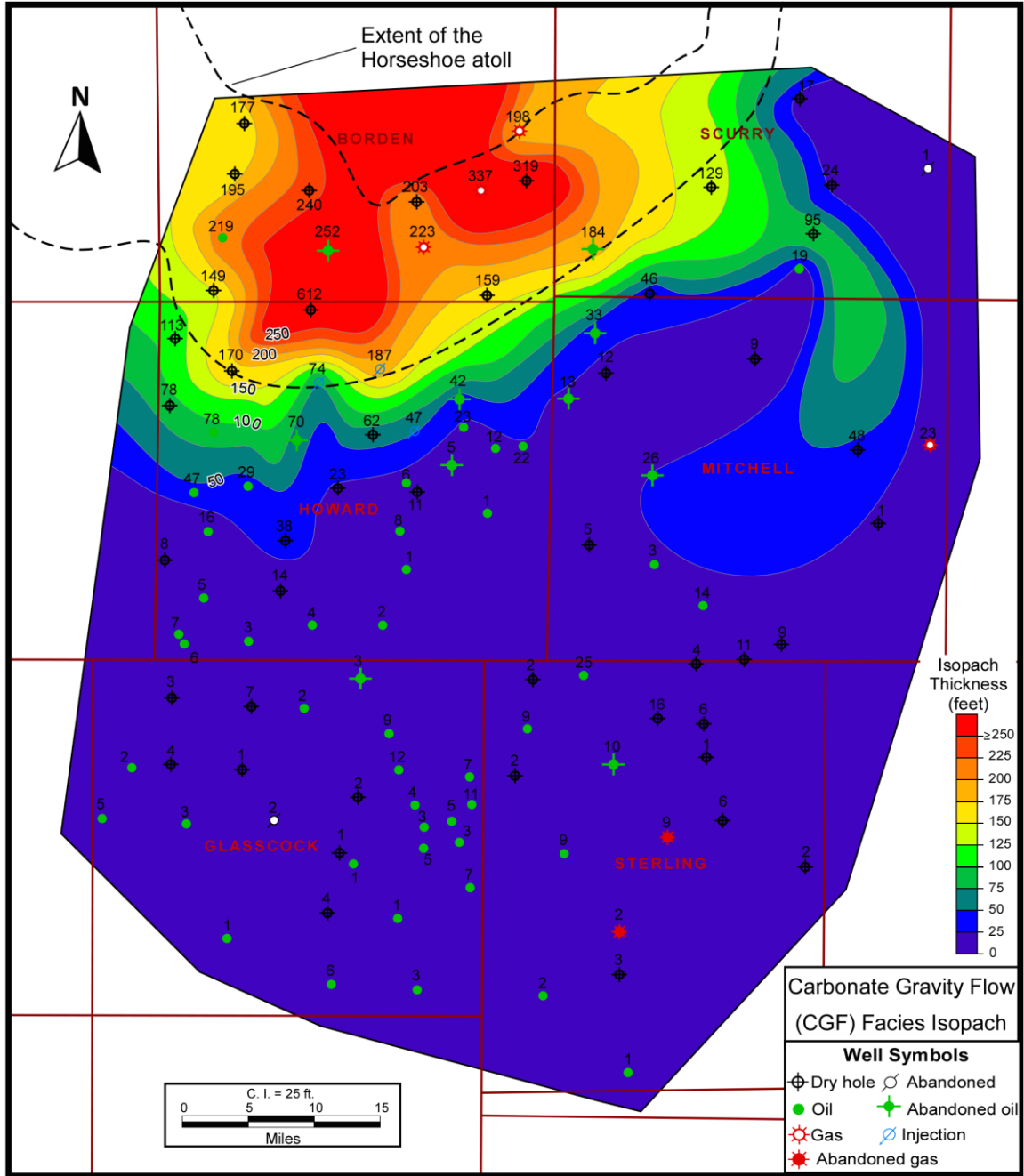


Figure 14. Carbonate Gravity Flow (CGF) facies cumulative isopach map. The distribution of this facies correlates closely with the position of the Horseshoe Atoll. The corresponding trend is disrupted in central to southeastern Scurry County and northeastern Mitchell County where the facies extends basinward as an elongate protrusion. The outline of the Horseshoe Atoll is depicted by the dashed black polygon in the northern portion of the study area. The position of the Horseshoe Atoll is modified from Vest Jr. (1970).

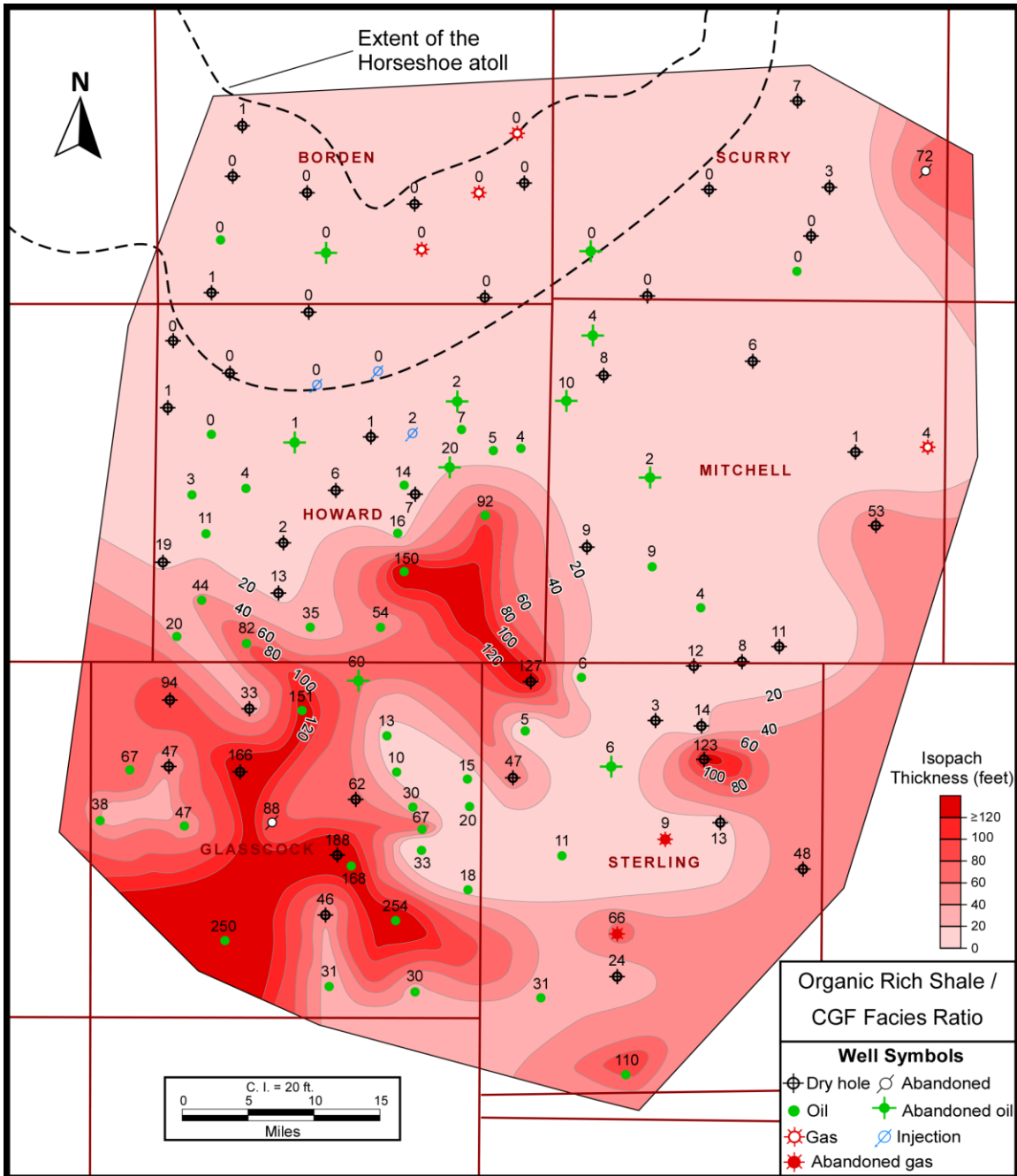


Figure 15. Organic Rich Shale (ORS)/Carbonate Gravity Flow (CGF) facies ratio isopach map. The ratio of ORS to CGF generally increases basinward away from the Horseshoe Atoll. The outline of the Horseshoe Atoll is depicted by the dashed black polygon in the northern portion of the study area. The position of the Horseshoe Atoll is modified from Vest Jr. (1970).

## CHAPTER SIX

### Depositional History

In response to an acceleration in sea level rise during the Late Desmoinesian, strata of the Horseshoe Atoll evolved from an aggradational to retrogradational succession with a broad, pinnacle-style geometry, and culminated in a “drowned unconformity” (*sensu* Schlager 1992) during the early Permian (Adams, 1962; Vest, Jr., 1970; Greenlee and Lehman, 1993).

Variability in the succession of facies within basinward-equivalent strata to the Horseshoe Atoll are characterized by a transition from carbonate to siliciclastic dominated basinal facies. The prevalence of the carbonate CGF facies (Figure 14) is most prevalent in areas within and proximal to the atoll, while the siliciclastic-enriched ORS and NRS facies (Figure 12, Figure 13) are most prevalent in areas distal to the atoll. During aggradational to retrogradational growth of the atoll, carbonate sediments were readily supplied to adjacent basinal areas via sediment gravity flows, possibly induced by bank top and slope destabilization during lowstands in sea level, e.g., CGF distributions in Scurry and Mitchell counties (Figure 14) (*sensu* Greenlee and Lehman, 1993). Regardless of mechanism, basinal stratigraphic successions that are dominated by sediment gravity deposits have diluted concentrations of organic matter, and therefore, lower exploration potential.

Upon drowning of the atoll, the supply of carbonate sediment was shut off and resulted in a proportional increase in siliciclastic sediments.

This transition from basinal carbonates to siliciclastics coincides with the Three Fingers stratigraphic top, and is conspicuous in wells proximal to the atoll (Figure 16). Organic enrichment of basinal shales above the Three Fingers generally increases with increasing distance away from the atoll (Figure 12, Figure 16). Some basinal wells show no increase, and in some cases show a decrease in the proportion of ORS above the Three Fingers. This is particularly evident in relation to the Eastern Shelf where there is a relative decrease in the ORS facies proportion in the proximal areas. This may suggest that clastic input from the shelf diluted organic richness in adjacent areas (see cross sections D-D' through F-F' Appendix D).

In summary, the highest concentration of the ORS facies, and therefore the greatest exploration potential, is located in the basin center in Howard and Glasscock counties (Figure 12). The least prospective areas for Cline exploration are those proximal to the Horseshoe Atoll, Eastern Shelf, and the inferred lowstand channel, i.e., Borden, Scurry, Mitchell, and Sterling counties (Figure 14).

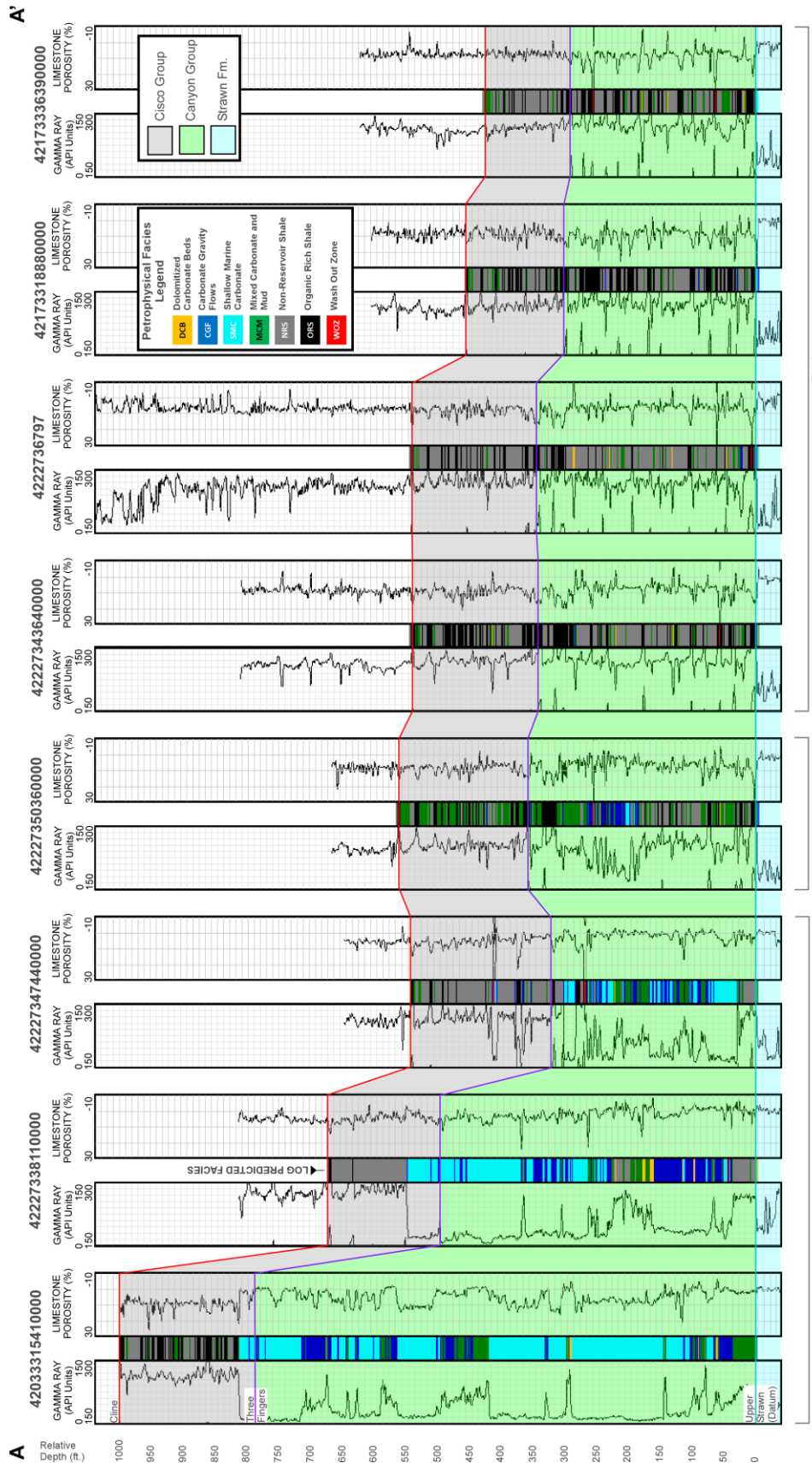


Figure 16. Simplified cross-section A-A' illustrating the stratigraphic relationships of the Strawn, Canyon and Cisco groups across the study area. The location of the cross-section is shown on Figure 5. Petrofacies distributions are based on the transform of Crass (2015) and are displayed within the depth track of each well log (petrofacies color codes are provided in the legend).

## CHAPTER SEVEN

### Conclusions

1. The Cline interval encompasses the Pennsylvanian Canyon and Cisco Groups and is comprised of eight depositional facies that accumulated in slope (LCM, MSC, LCF, GSC, IGC) and basinal (BLM, MBM, SBM) environments.
2. A distribution of seven petrophysical facies from Crass (2015) were assessed in this study. Five of these facies (DCB, CGF, MCM, NRS, and ORS) were derived from data compiled from core descriptions and petrophysical data. Two additional facies (WOZ and SMC) account for both the occurrence of borehole wash out zones (WOZ) and presence of shallow marine carbonates of the Horseshoe Atoll (SMC).
3. The most prospective unconventional reservoir is the ORS facies (average TOC of 4.5%). Sedimentological and ichnological features of the ORS facies suggest deposition in an oxygen-depleted offshore marine environment. This facies is most abundant in Glasscock County and the southern portion of Howard County.
4. The occurrence of the ORS facies is influenced by proximity to physiographic features such as the Horseshoe Atoll, Eastern Shelf, and the lowstand channels cut into northeastern portions of the atoll in the SACROC and Cogdell field areas in Scurry County. Carbonate gravity flows derived from the Horseshoe Atoll dilute organic richness and reduce unconventional shale reservoir quality. This effect is amplified when channels are present that deliver sediment gravity flow deposits further into the basin.

5. Organic enrichment of basinal shales above the Three Fingers generally increases with increasing distance away from the Horseshoe Atoll and Eastern Shelf.

## APPENDICES

## APPENDIX A

### Structure Maps

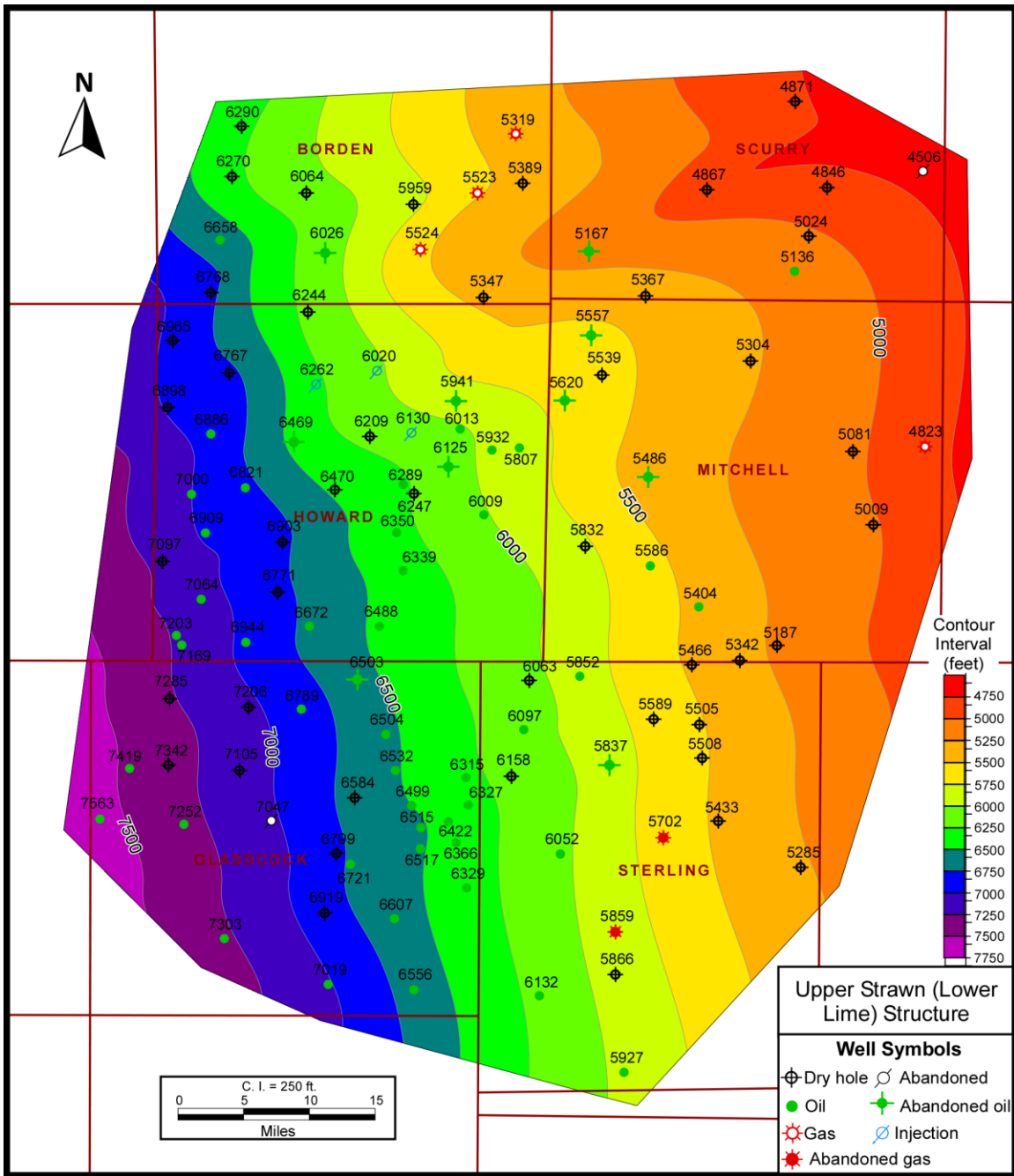


Figure A 1. Upper Strawn (Lower Lime) structure map.

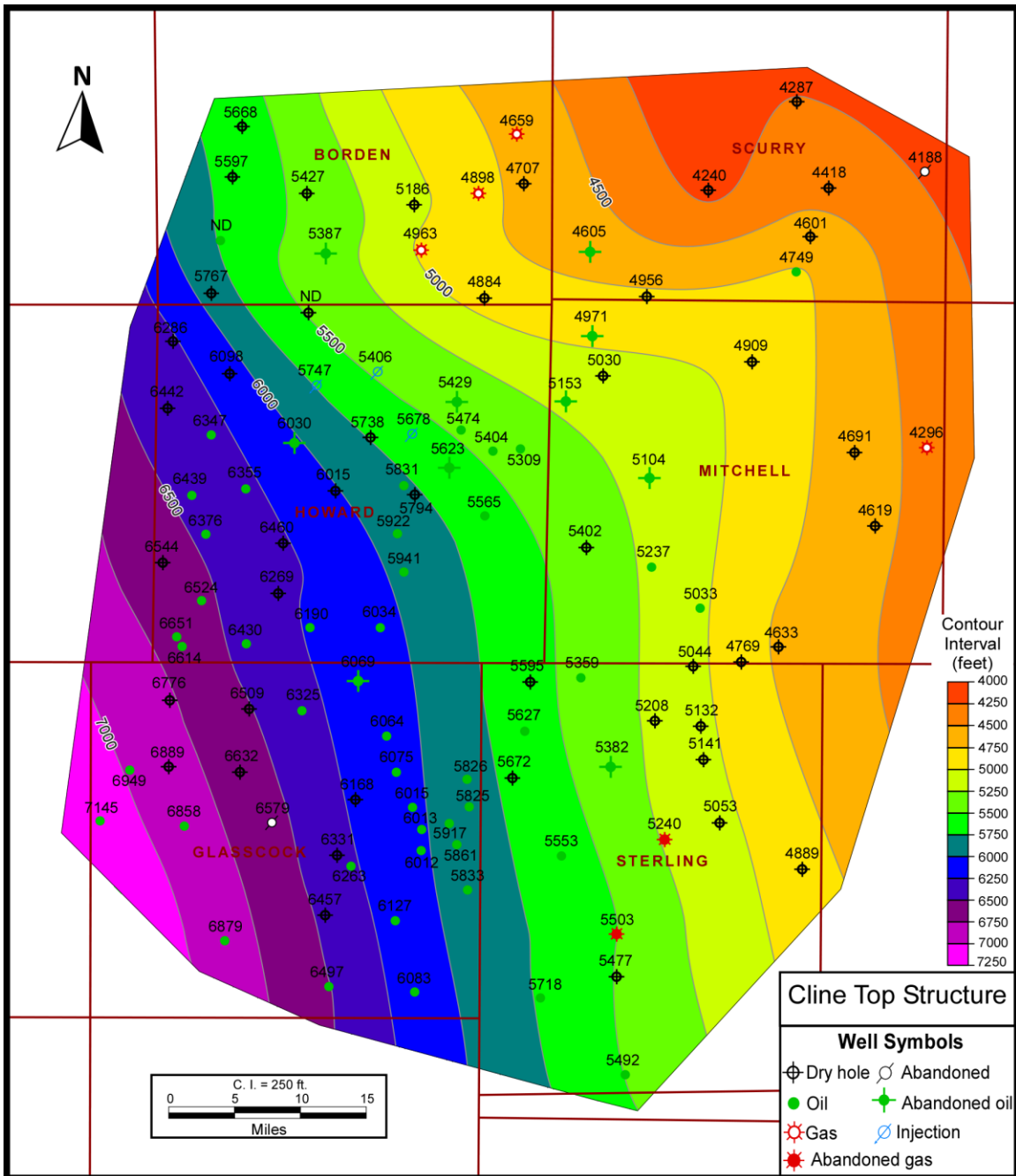


Figure A 2. Top Cline structure map.

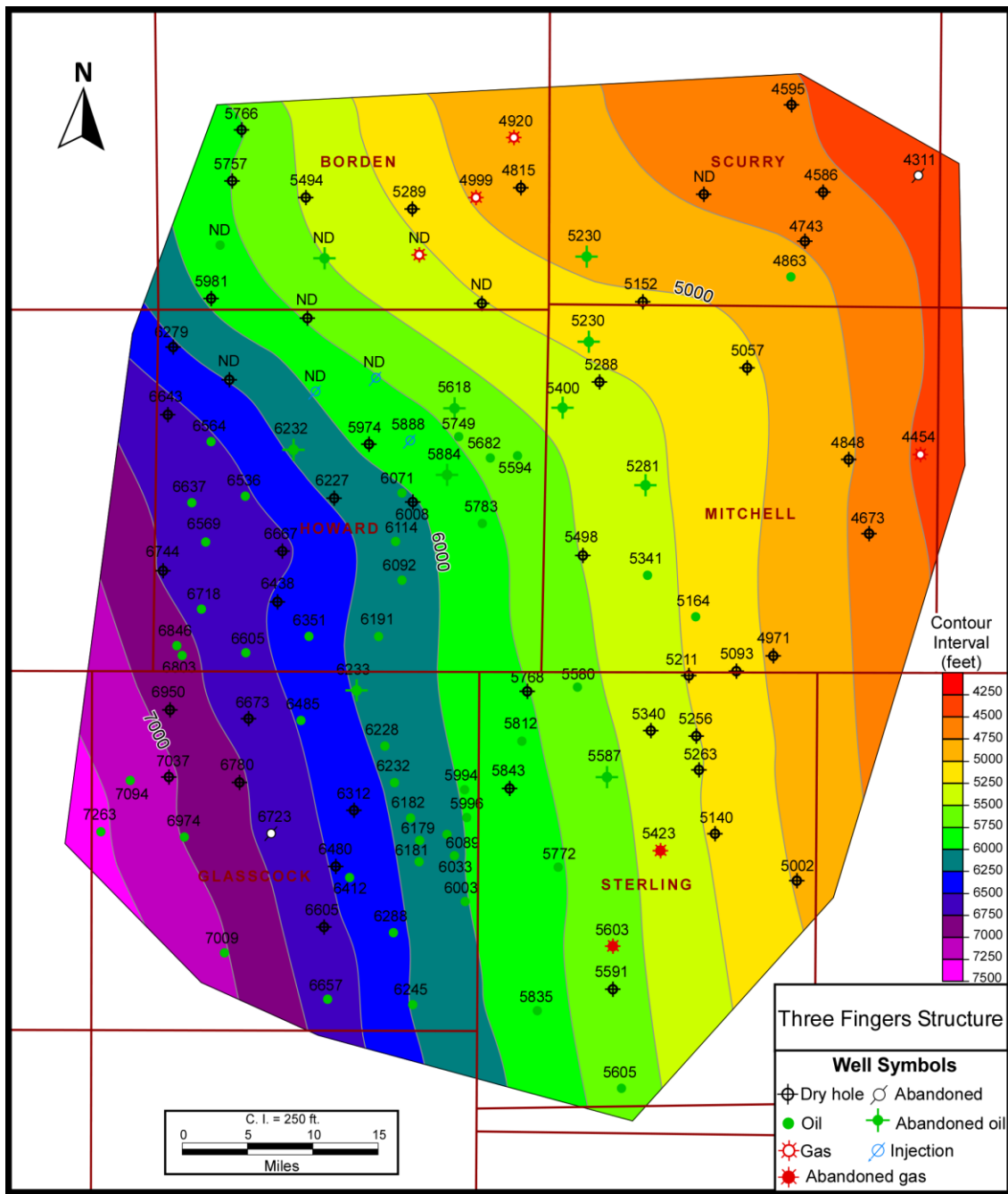


Figure A 3. Three Fingers structure map.

APPENDIX B

Facies Isopach Maps

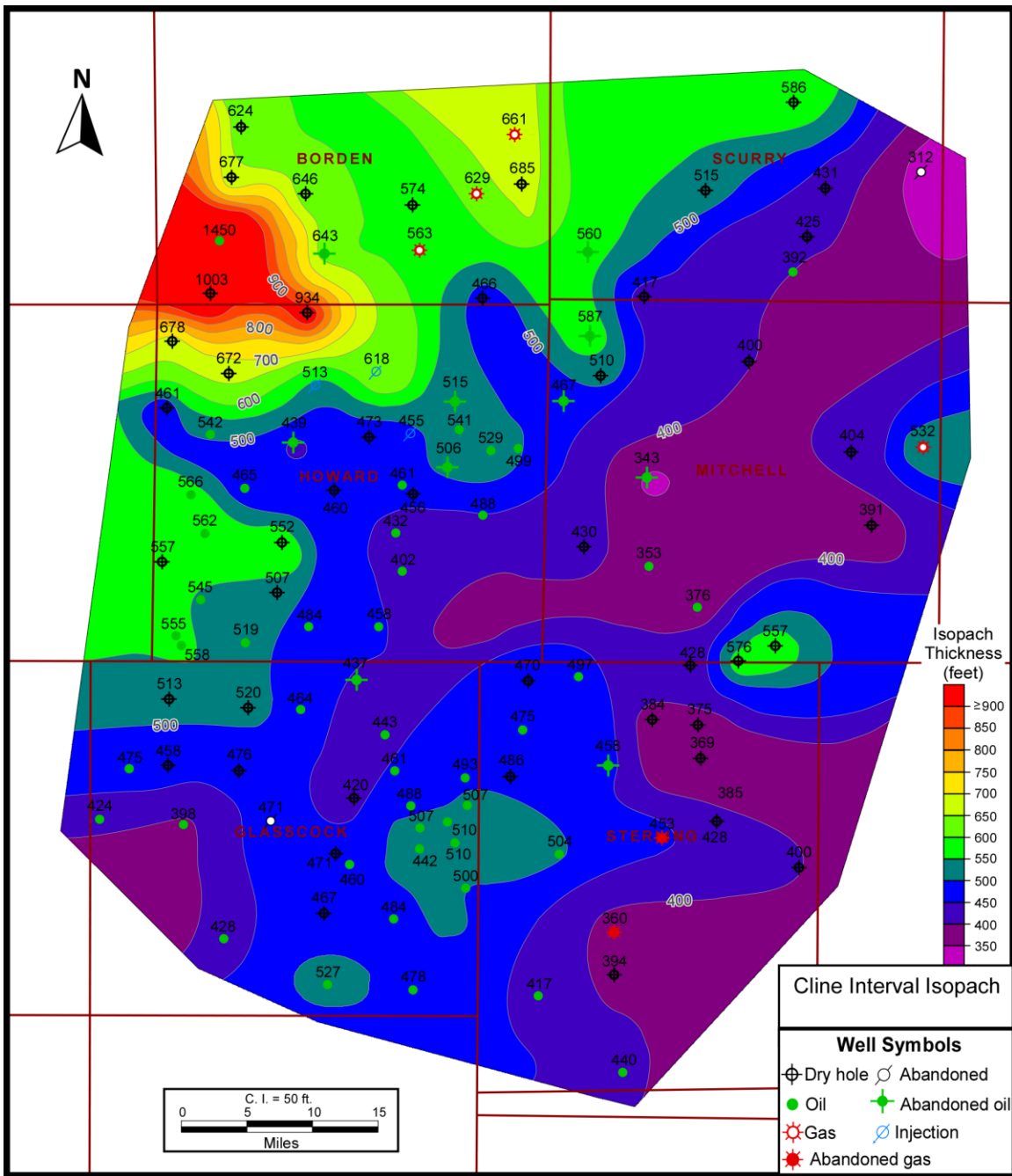


Figure B 1. Cline interval isopach map.

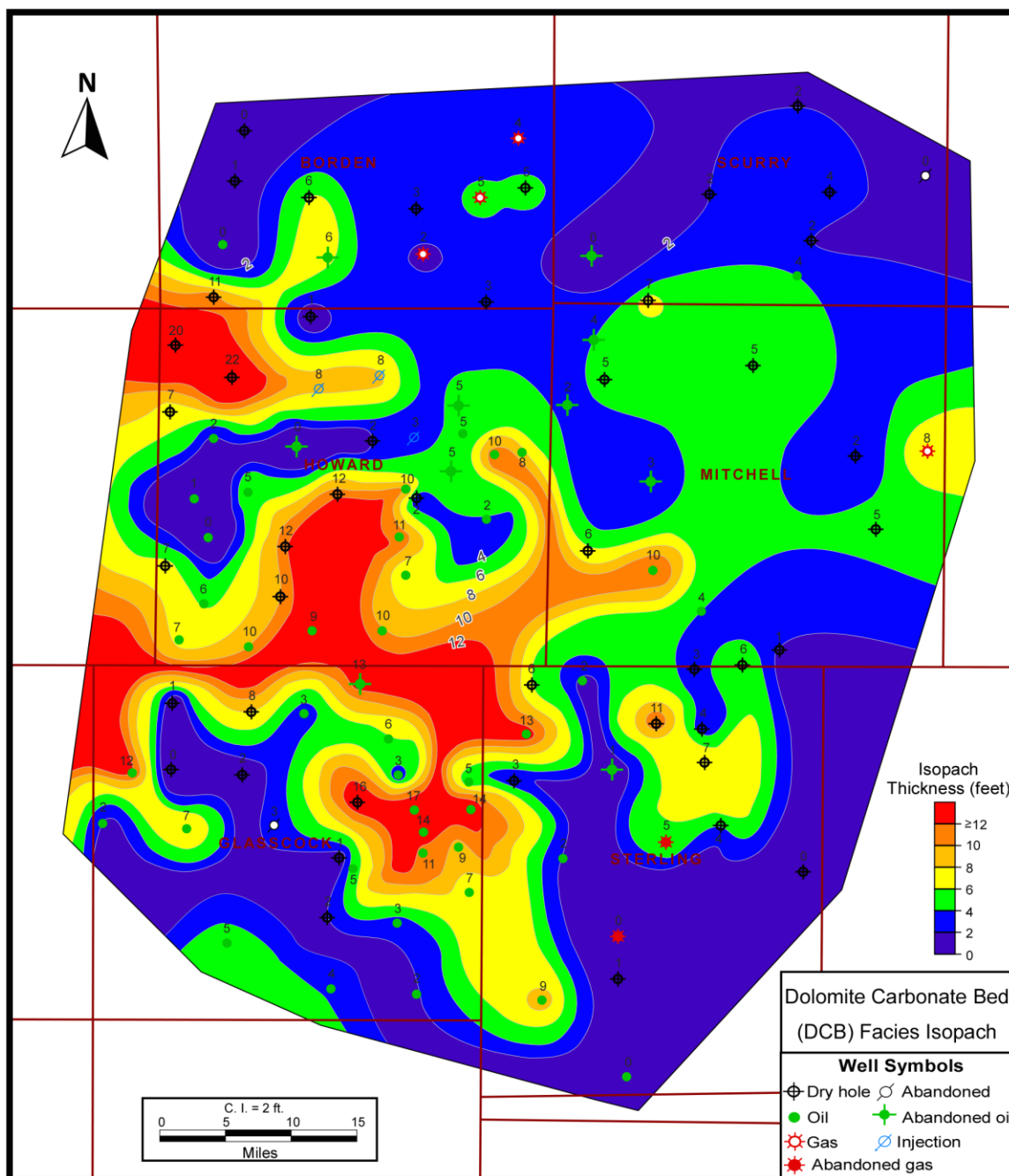


Figure B 2. Dolomite Carbonate Bed (DCB) facies cumulative isopach map.

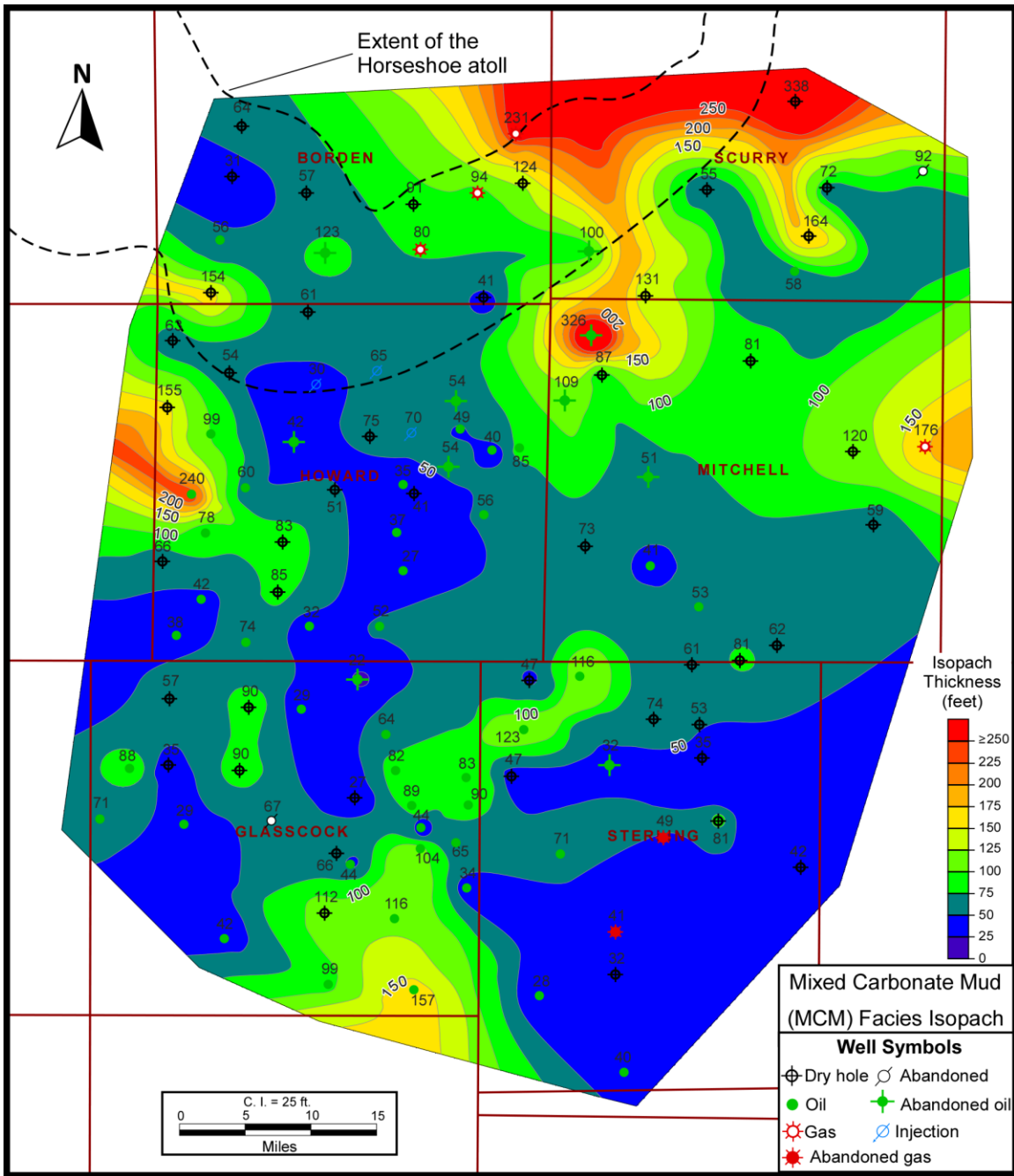


Figure B 3. Mixed Carbonate Mud (MCM) facies cumulative isopach map.

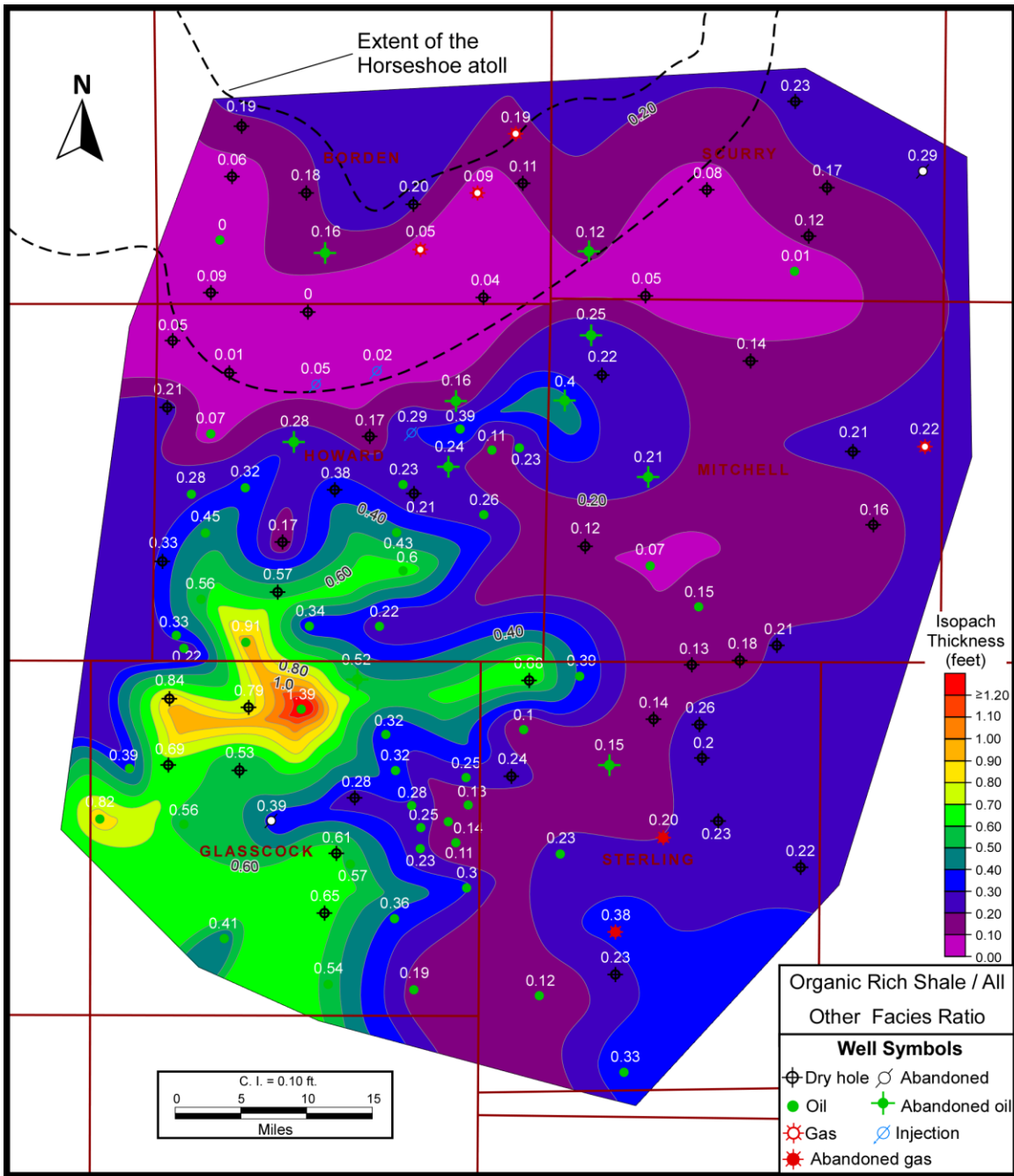


Figure B 4. Organic Rich Shale (ORS) / All Other Facies ratio isopach map.

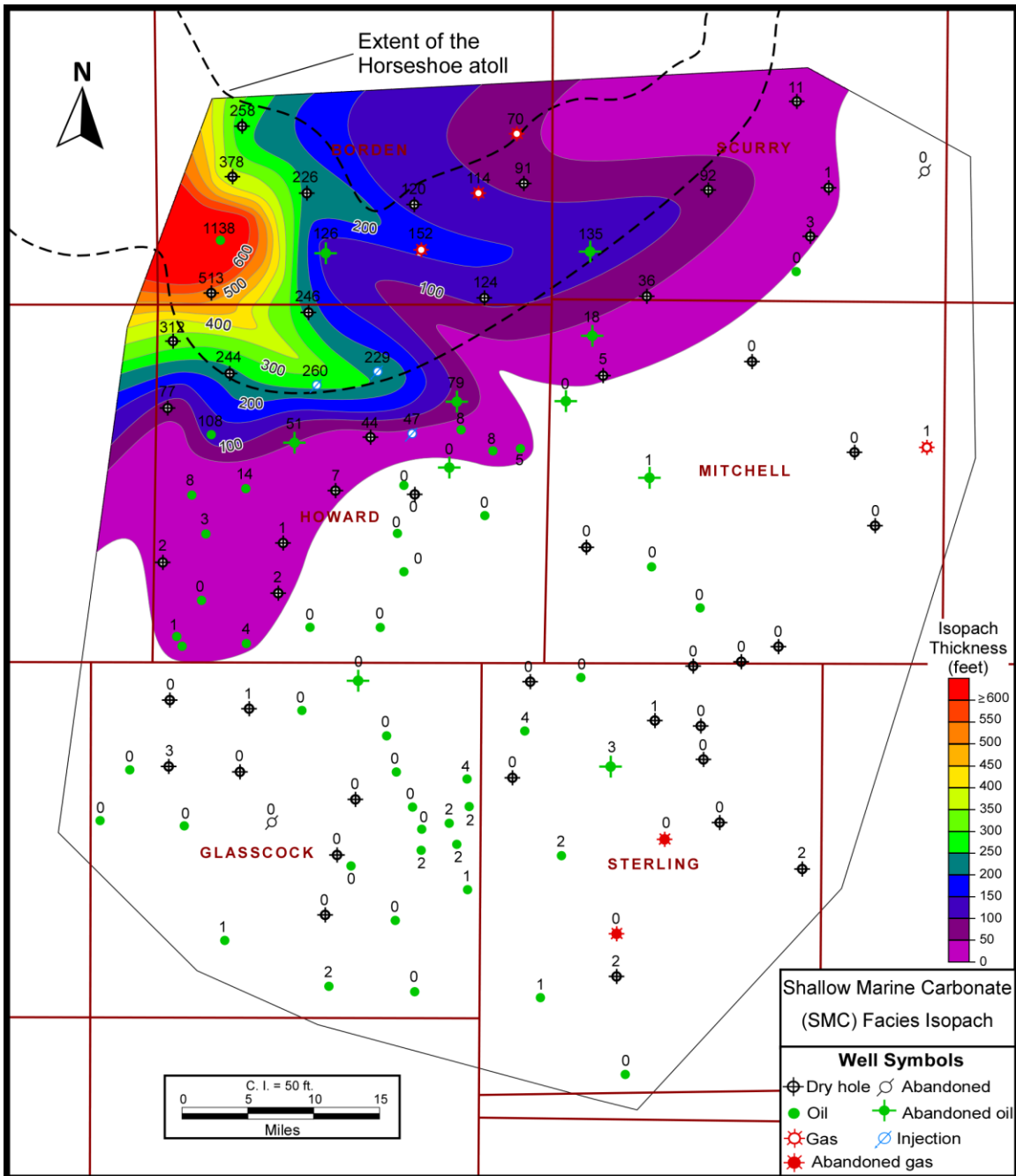


Figure B 5. Shallow Marine Carbonate (SMC) facies cumulative isopach map.

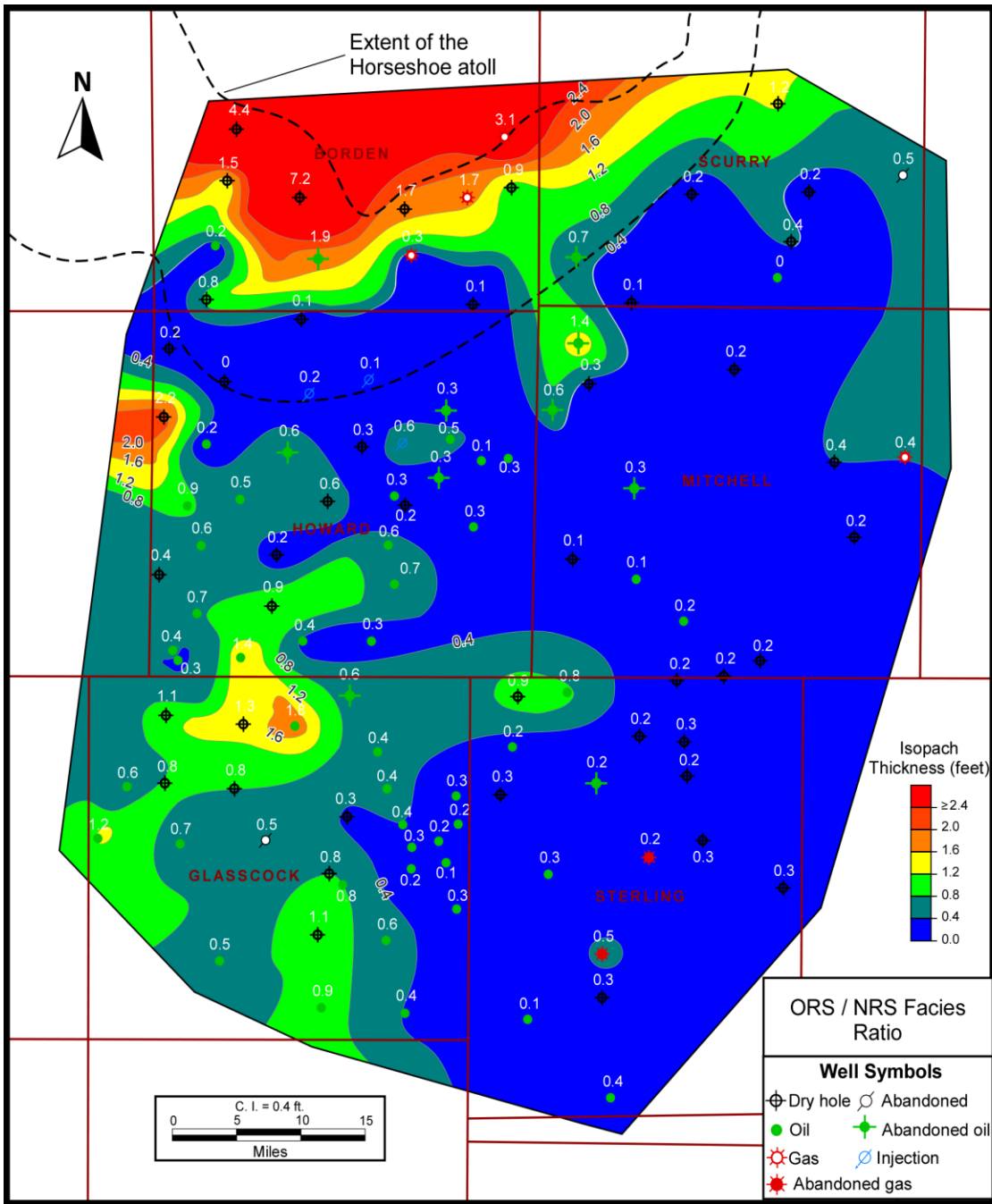


Figure B 6. Organic Rich Shale (ORS) / Non Reservoir Shale facies ratio isopach map.

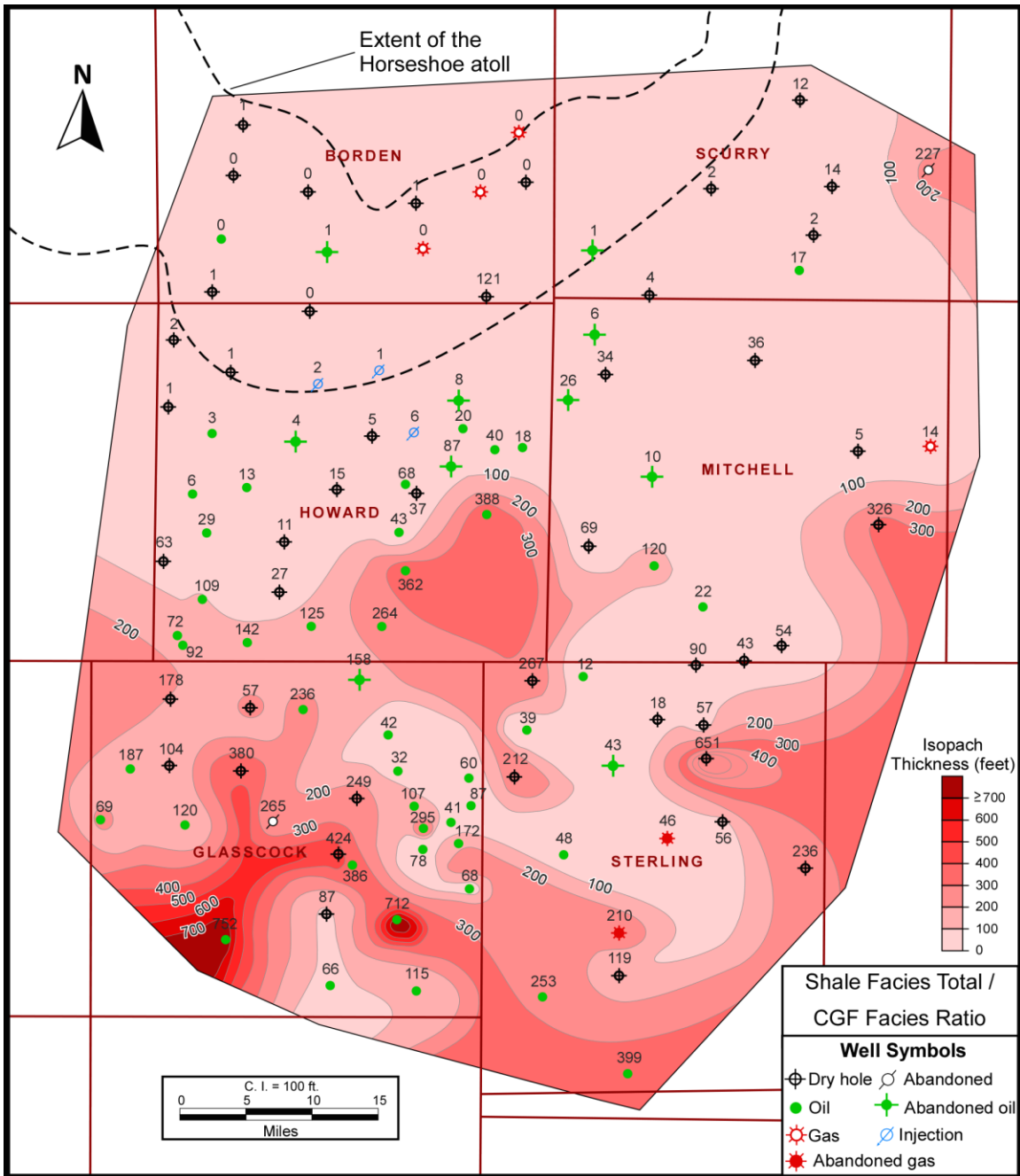


Figure B 7. Shale facies total (ORS+NRS)/Carbonate Gravity Flow (CGF) facies ratio isopach map.

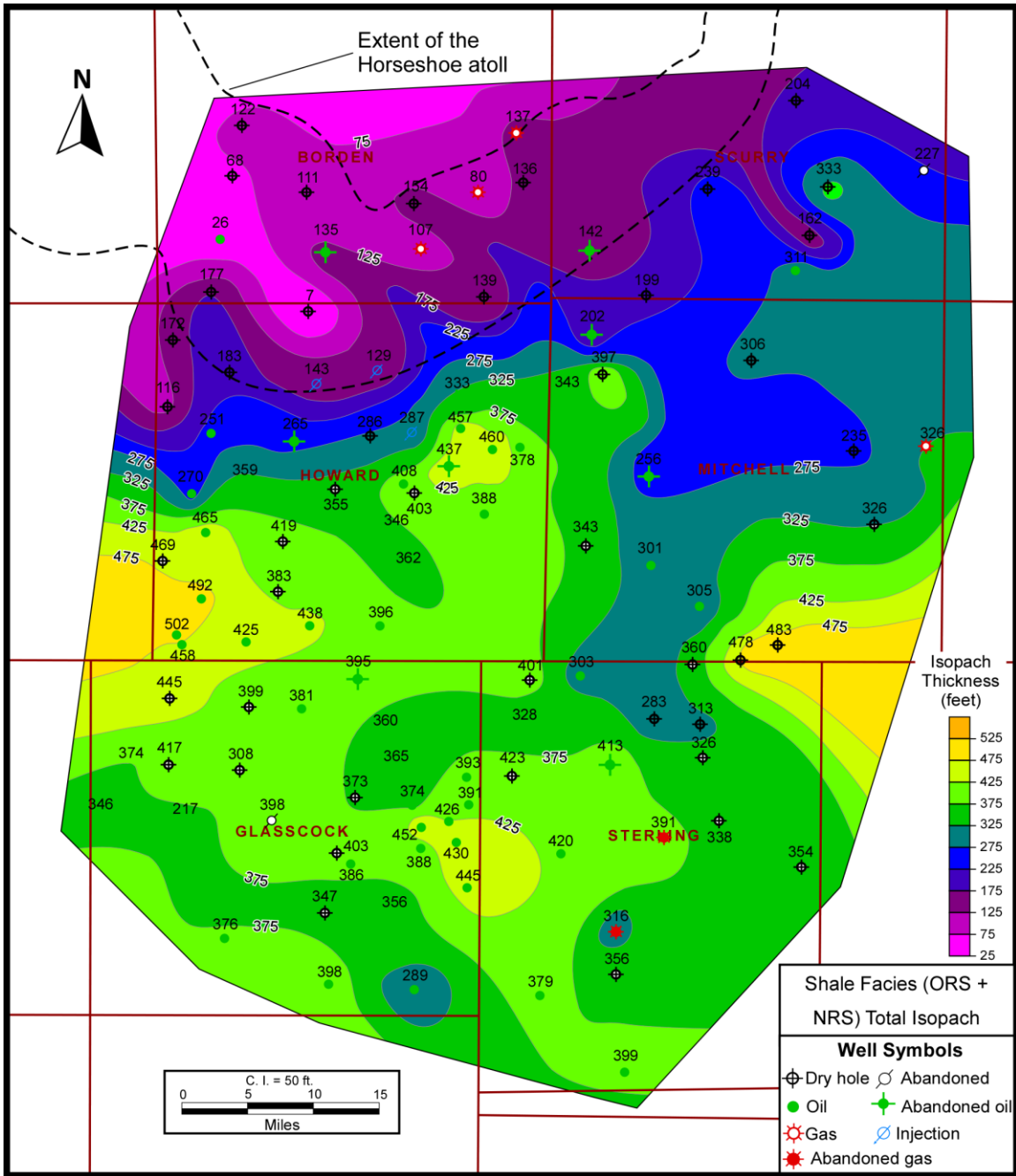
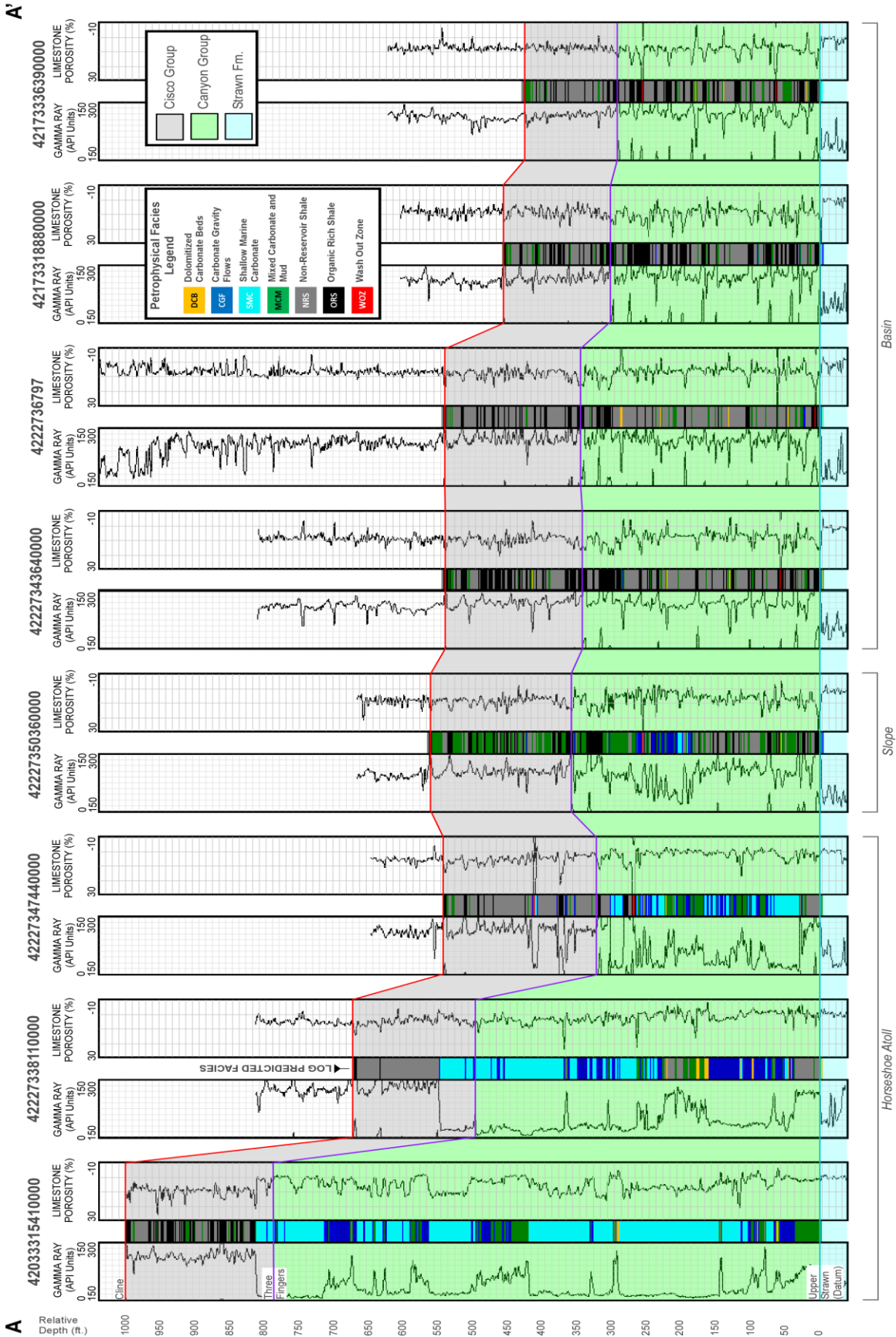
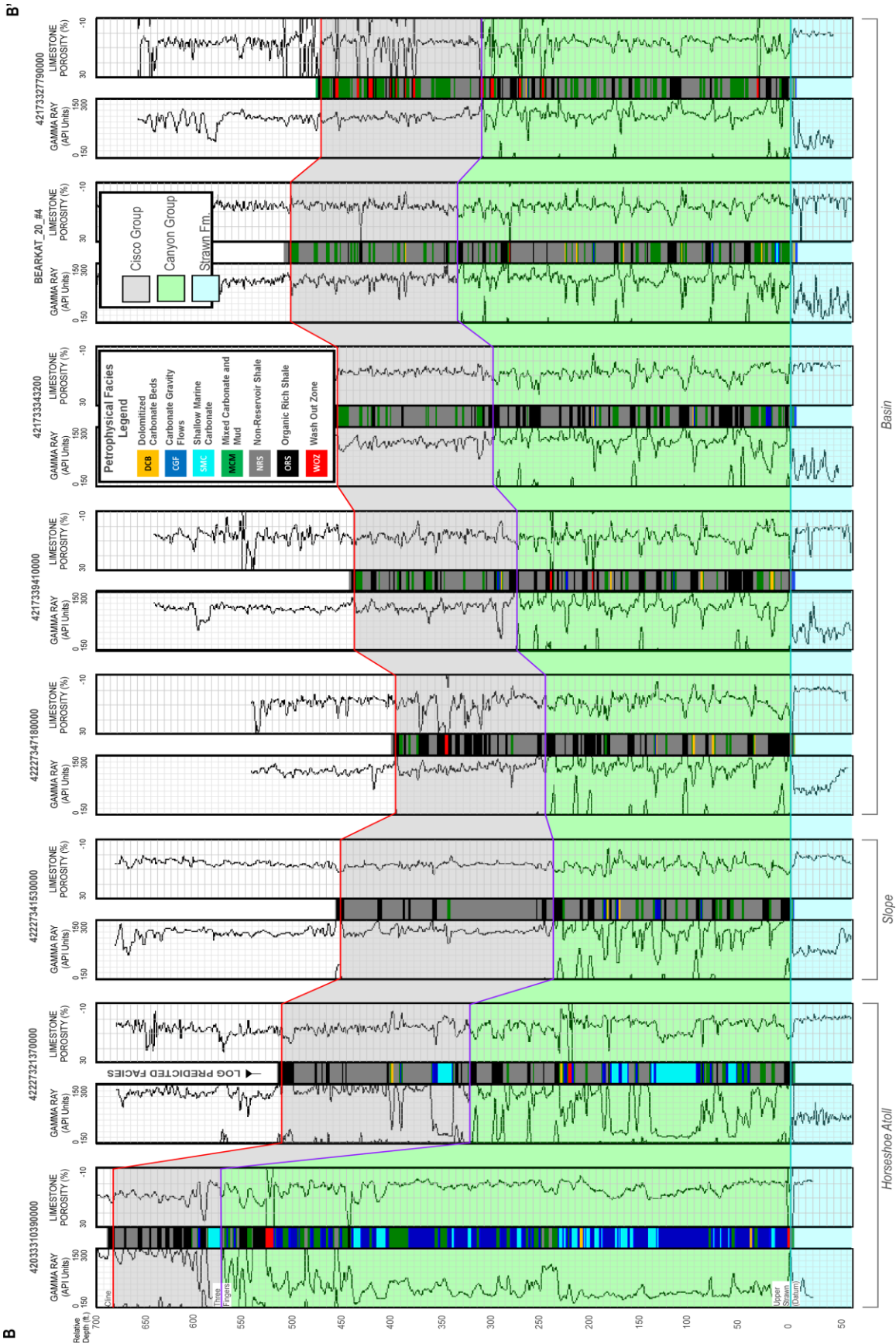


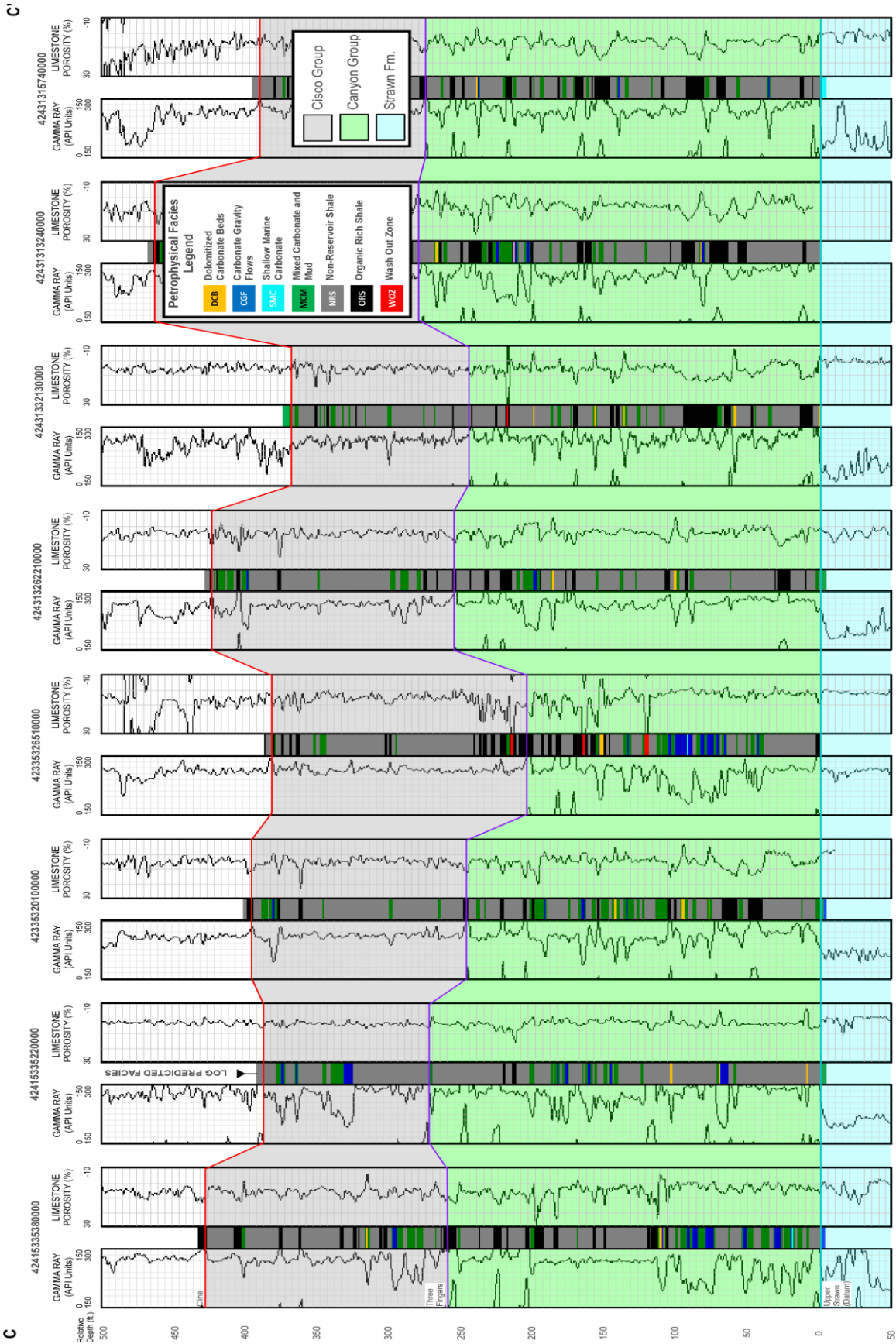
Figure B 8. Organic Rich Shale (ORS) + Non Reservoir Shale (NRS) facies ratio isopach map.

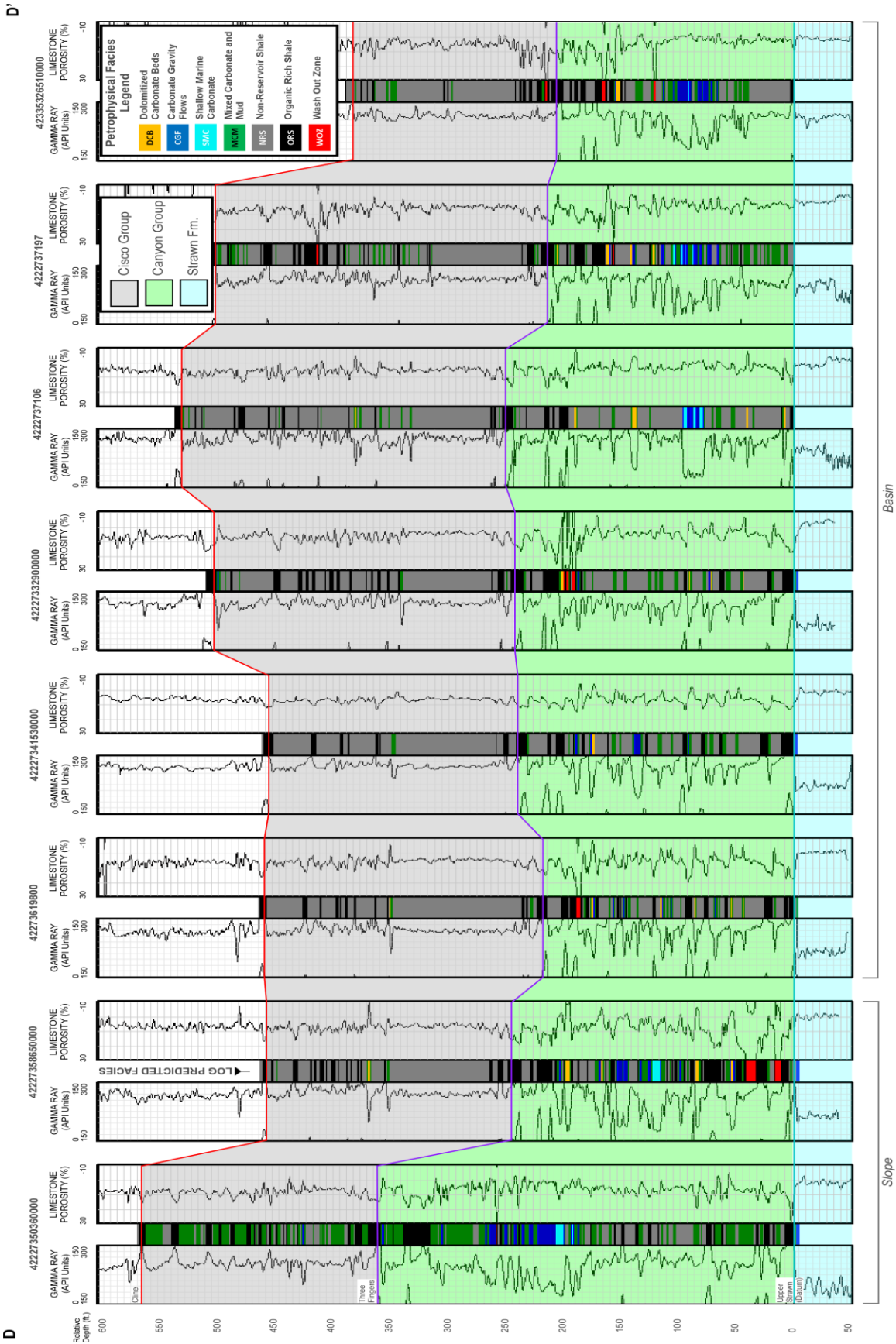
## APPENDIX C

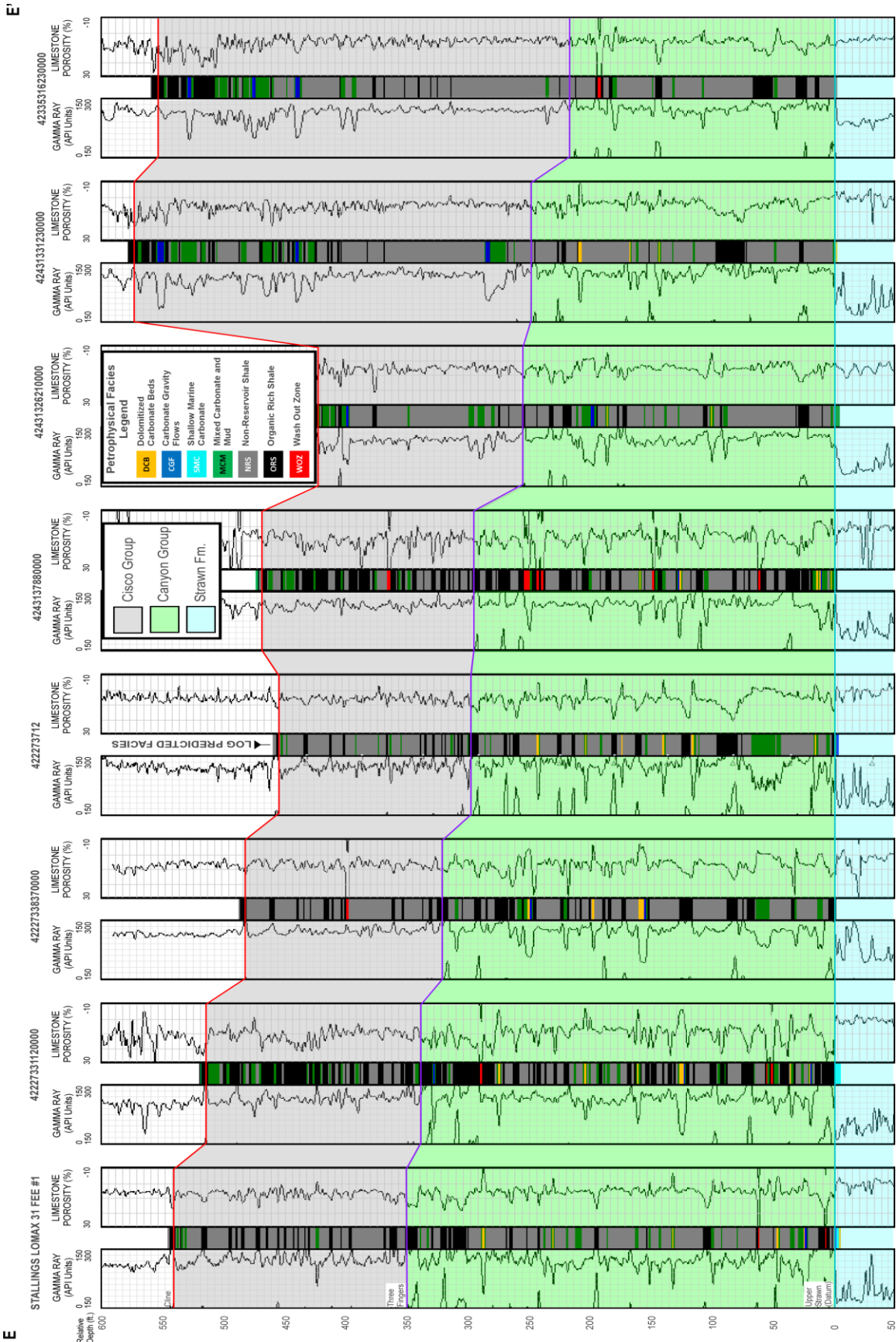
### Cross-Sections





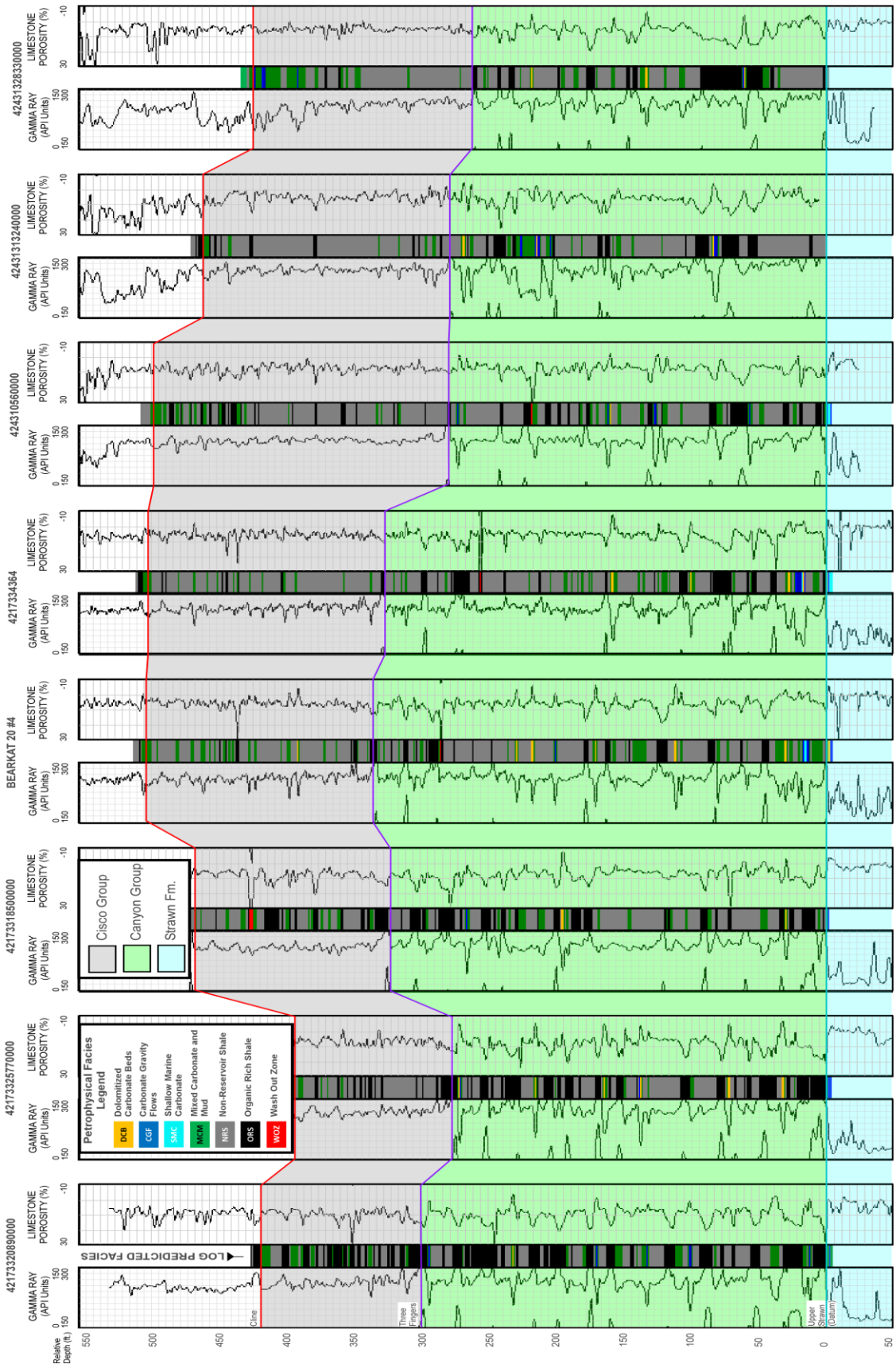






F

F



APPENDIX D

Core Description Forms

## Core Description Legend

### Sedimentary Structures and Grain Types

 Planar Laminations	 Brachiopod/Bivalve
 Wavy Laminations	 Bryozoan
 Normal Grading	 Gastropod
 Inverse Grading	 Lithoclast
 Crinoid	 Intraclast
 Fusulinid	 Phosphate Nodule

### Ichnofabric Index

- 1 – No bioturbation recorded; all original sedimentary structures.
- 2 – Discrete, isolated trace fossils; up to 10 percent of original bedding disturbed.
- 3 – Approximately 10 to 40 percent of original bedding disturbed. Burrows are generally isolated, but locally overlap.
- 4 – Last vestiges of bedding discernible; approximately 40-60 percent disturbed. Burrows overlap and are not always well defined.
- 5 – Bedding is completely disturbed and sediment is nearly or totally homogenized.

### Fractures

Fractures tabulated on a per-foot basis in bins of 5. Unless otherwise indicated, fractures are bedding plane fractures and separations.

| Centerline Fracture

∩ Petal Fracture

### Effervescence

- 0 – No reaction. Negligible calcite fraction.
  - 1 – Weak reaction. Low proportion of calcite.
  - 2 – Moderate reaction. Subequal proportions of calcite and other minerals.
  - 3 – Strong reaction. Primary mineral is calcite.
- Dolo – Weak reaction unless powdered. High proportion of dolomite.

### Color

Color designations assigned on a per-foot basis using direct visual comparison to Munsell Soil Color Charts (2009). Unless otherwise noted, colors are from hue chart "GLEY 2."

Depth	CO <sub>3</sub> Texture					Facies	Grains	Sed. Struc.		Grain Size (mm)	Dry Color	Fracture		Photo	Effervescence	Comments
	M	W	P	G	B			Mech.	I.I.			Freq.	Cement			
8000						LCF		1	9	5/10B	5			3	Debris Flow few calcos Healed Frac. Vert to sub vert.	
						BLM		1			10			3		
								2			15			1		
								3			15			1		
								3			15			1		
								3			15			1		
								3		3/5PB	15			1		
						SSM		3			15			1		
								2			20			1		
						BLM		2			20			0	Single V. Fracture / calcos	
								4			20			1		
								4			20			2		
								4		3/5PB	15			2		
								4			15			1		
						MBM		4		4/5PB	15			1		
								2			25	None		1		
						BLM		2			25	Calcs		1	Some subhorizontal Healed Fract.	
								3			20			2		
						SSM		3		3/5PB	20			2	unloading fract	
								5			15			1		
						MBM		5		4/5PB	10			1	Fractures Natural	
								4			5			3		
						SBM		4		4/10B	5			2	TA	
						MSC		4		4/5PB	5			2		
								4			10			2		
								4		3/5PB	15			2	Fine grained skeletal Heals	
						SBM		4			15			2		
						LCF		4		4/5PB	10			2	Debris Flow Grain Flow Debris Flow TC	
						IGL		4		3/5PB	10			2		
						LCF		4		4/5PB	10			2		
						SSM		4		3/5PB	15			2	Fractures = to bedding, look like unloading Fractures	
								1			20			2		
								1			20			1		
						BLM		1			20			1		
8040						SBM		4		4/5PB	20	None		2		

M W F M C  
SiO<sub>2</sub> Texture

Core diameter = 4"

Imperial Units (1" = 5')

Project/Location:

Logged By:

Date:

Page 2 of 10

Depth	CO <sub>3</sub> Texture					Clastic	Facies	Grains	Sed. Struc.		Grain Size (mm)	Dry Color	Fracture		Photo	Effervescence	Comments
	M	W	P	G	B				Mech.	LI.			Freq.	Cement			
7960							MBM	○ ○ ○		1	3/5PB	10			1/2		
							LCF	○ ○ ○		1	5/5PB	10			3		
							LCF	○ ○ ○		1	5	5/5PB	5		3		Debris Flow
7965							SBM	○ ○ ○		4	4	15			1		
							MBM	○ ○ ○		4	4	20			1		
							LCF	○ ○ ○		1	25	3/5PB	10		M1/C3		
							LCF	○ ○ ○		1	4	4/5PB	10		M1/C3		
							GSC	○ ○ ○		1	4	6/5PB	10		3		TA-T3
7970							GSC	○ ○ ○		1	2	5			3		← 1cm BLM
							LCF	○ ○ ○		1	12	5/5PB	5		3		TA ← contact in BLM
							GSC	○ ○ ○		1	2	2	10		3		Debris Flow
							MBM	○ ○ ○		2	2	10			3		← contact has 1 in SBM
7975							MBM	○ ○ ○		3	2	10			3		TA healed fract + dead o.l.
							GSC	○ ○ ○		3	2	15			2-3		TA → Fractured
							MBM	○ ○ ○		3	2	4/5PB	15		3		
							GSC	○ ○ ○		1	4	3/5PB	20	CaCO <sub>3</sub>	3		TA
							MBM	○ ○ ○		3	3	4/5PB	20		3		TA
7980							GSC	○ ○ ○		1	3	5/10B	15	CaCO <sub>3</sub>	3		TA, sub-V Healed Frac
							MBM	○ ○ ○		3	3	10			3		
							MBM	○ ○ ○		3	3	5			3		
7985							MBM	○ ○ ○		1	4	4/5PB	10		3		Debris Flow
							LCF	○ ○ ○		1	10	5/5PB	5		3		
							SBM	○ ○ ○		4	4	4/5PB	15		1		
7990							T	○ ○ ○		4	4	3/5PB	18		1		
							MBM	○ ○ ○		4	4	4/5PB	10	SiO <sub>2</sub>	0		Large chert last in block are healed fractures + open fracs Multi-directional fractures → 2 V. Healed frac
							LCF	○ ○ ○		4	3	5/5PB	3	Calc	0/3		
							LCF	○ ○ ○		11	11	5/10B	1		3		
7995							LCF	○ ○ ○		1	2	2-5/5PB	20		3		
							LCF	○ ○ ○		1	15	15			2		
							LCF	○ ○ ○		1	15	15			1		
8000							SBM	○ ○ ○		3	3	3/5PB	15		1		

M W F Md C  
SiO<sub>2</sub> Texture

Core diameter = 4"

Imperial Units (1" = 5')

Project/Location:

Logged By:

Date:

Page 3 of 10

Depth	CO <sub>2</sub> Texture					Clastic	Facies	Grains	Sed. Struc.		Grain Size (mm)	Dry Color	Fracture		Photo	Effervescence	Comments
	M	W	P	G	B				Mech.	I.I.			Freq.	Cement			
7920							SBM	∅∅∅		2	3/5 PB	20					
								∅		3	4/5 PB	25					
								∇∅		3		20					
								∇∅		4	3/5 PB	15					
7925							MBM			4		10					
										4	5/4/1	15					
							IGC		↓6	1	4	5/10E	5		3	2 Ig. Grain Flows	
							GSC	∅∅∅		1	5	5/5 PB	10		3	TA	
							MBM	∅		4	5/4/1	5			2	1 long Vertical Fracture	
7930							SBM	∇∅∅		3		20					2 in debris flow 20'
							LCF	∅∅∅		3		10				3	Debris Flow
										12		20					
												20					
7935												20					
												20					
							SBM	∇∅∅				20					
												20					1 in T <sub>D</sub> → lime mud
												20					
7940							SBM					25					
												20					
							RLM					20					
							LCM					20					TDE
												10					
												5					
7945							LLF	∅∅∅				3					Debris Flow
												5					
												15					
												30					
7950							SCM	∅∅∅				30					
												30					
												30					
												20					
												15					
												5					
							GSC	∇∅		16	19	5/5 PB	5	Calcs			Sub vert + horizontal healed frac
							SBM	∇∅		4		15					
							LCM	∅∅∅		1		25/5 PB	15				
7955							LCF	∅∅∅		2		6	5/5 PB				Debris Flow followed by T <sub>D</sub> (lime)
							SBM	∇∅		4		15					
							MBM	∇∅		4		20					
							LCF	∅∅∅		1	5	15					
7960							MBM	∇∅∅		5		15					

M V F M C  
SiO<sub>2</sub> Texture

Core diameter = 4"

Imperial Units (1" = 5')

Project/Location:

Logged By:

Date:

Page 4 of 10

Depth	CO <sub>2</sub> Texture					Facies	Grains	Sed. Struc.		Grain Size (mm)	Dry Color	Fracture		Photo	Effervescence	Comments
	M	W	P	G	B			Mech.	I.L.			Freq.	Cement			
7880																
7885							○			10f 10f 3/5PB 16f 2.55PB 10				0	Broken up	
7890							○			3/5PB 10f 4/5PB 10 3/5PB 10				0		
7895						BLM	●			10f 10f 10f 10f 5f 3/1 15 5f 2/1 10 5f 2.5/1 10				0	V-healed V-healed Horizontal Healed	
7900						BLM	○			4/5PB 20 25 3/10PB 30 25 4/10PB 30 3/10PB 25				0	Highly Fractured up	
7905						SBM LCF LCM LCF	○ ○ ○ ○			5f 1/1 10 7 3 8 4/10PB 3				1	Dolomite Dolomite Dolomite	
7910										3/5PB 20 4/5PB 20 3/5PB 20 Totally fractured				1	4 in ID (lime)	
7915										4/5PB 20 3/10PB 20 20 4/5PB 15				2		
7920						SBM BLM SBM	○ ○ ○			3/5PB 10 2.55PB 10 20 3/5PB 15				1	Very black,	

M W F Md C  
SiO<sub>2</sub> Texture

Core diameter = 4"

Imperial Units (1" = 5')

Project/Location:

Logged By:

Date:

Page 5 of 10

Depth	CO <sub>3</sub> Texture				Carb. Clastic	Facies	Grains	Sed. Struc.		Grain Size (mm)	Dry Color	Fracture		Photo	Effervescence	Comments
	M	W	P	G				Mech.	I.I.			Frac.	Cement			
7840								3			15			1		
								3			4/5 PB			1		
								3			3/5 PB			1		
								3			15			1		
7845						MBM	0 ∇ ∅	3			4/5 PB			1		Belemnite? ⇐
								1			15			0		
								1			15			0		
7850								1			15			0		Small lime TDs
								1			15			0		
								1			15			0		
7855								1			3/5 PB			0		
								1			15			0		
								1			15			0		
								1			15			0		
								1			15			0		
						BLM		3			2.5/5 PB			0		Very Black
								3			15			1		.5" TDs → lime mud
7860						SBM		3			3/5 PB			1		
						MSL		1			4/5 PB			1		Dolomite bed, no bedding preserved
								3			15			1		Healed V.H. Fracts
								3			15			1		1" TDs → lime mud
						SBM		3			15			0		
								3			15			0		
7865								3			15			0		
								3			15			0		
								3			15			0		
								3			3/5 PB			0		
								3			2.5/5 PB			0		
7870								2			3/5 PB			0		
								3			2.5/5 PB			0		Broken up
								3			15			0		
						MBM		3			15			0		
								3			2.5			0		
7875								2			20			0		
								2			15			0		
								1			15			0		
								1			3/5 PB			0		V-Healed
								1			2.5/5 PB			0		
7880						BLM		1			3/5 PB			0		

M V F Md C  
SiO<sub>2</sub> Texture

Core diameter = 4"

Imperial Units (1" = 5')

Project/Location:

Logged By:

Date:

Page 6 of 10

Depth	CO <sub>3</sub> Texture				Ccarb. Clastic	Facies	Grains	Sed. Struc.		Grain Size (mm)	Dry Color	Fracture		Photo	Effervescence	Comments
	M	W	P	G				Mech.	I.I.			Freq.	Cement			
7800																
7805																
7810																
7815																
7820																
7825																
7830																
7835																
7840																

Tan phosphate nodules, possibly fluorapatite cemented

Lime T<sub>0</sub>

Lime T<sub>0</sub>

Lime T<sub>0</sub>

Lime T<sub>0</sub>

Terrigenous clay T<sub>0</sub> or wind delivered?

Lime T<sub>0</sub>

Healed V-Frac

M W F Md C  
SiO<sub>2</sub> Texture

Core diameter = 4"

Imperial Units (1" = 5')

Project/Location:

Logged By:

Date:

Page 7 of 10

Depth	CO <sub>3</sub> Texture				Carb. Classic	Facies	Grains	Sed. Struc.		Grain Size (mm)	Dry Color	Fracture		Photo	Effervescence	Comments
	M	W	P	G				B	Mech.			I.I.	Freq.			
7760							○ ∇	3		3	↑ 25				1	
								3		3	4/5 PB 25				1	
								3		3	3/5 PB 25				0	
								3		3	4/5 PB 25				1	
7765								3		3	↑ 25				1	
								3		3	3/5 PB 25				0	Broken up
								3		3	4/5 PB 25				0	
								3		3	↑ 25				1	
7770								3		3	25				1	
								3		3	3/5 PB 25				0	
								3		3	4/5 PB 25				0	
								3		3	3/5 PB 25				0	
								3		3	↑ 25				1	
7775								3		3	25				0	
								3		3	4/5 PB 25				1	
								3		3	3/5 PB 25				1	
								3		3	4/5 PB 25				1	
								3		3	↑ 25				1	
7780							∇	3		3	25				1	
								3		3	25				1	
								3		3	25				1	
								3		3	25				1	
								3		3	25				1	
7785								3		3	25				1	
								3		3	25				1	
								3		3	4/5 PB 25				1	
							●	3		3	3/5 PB 25				1	
7790							∇	3		3	↑ 25				1	
								3		3	25				0	
								3		3	25				0	
								3		3	25				0	
								3		3	25				1	
7795								3		3	4/5 PB 25				1	
								3		3	5/5 PB 25				1	
								3		3	4/5 PB 25				1	
								3		3	4/5 PB 25				1	
								3		3	4/5 PB 25				1	
7800							MPMT	3		3	4/5 PB 25				1	

M W F Md C  
SiO<sub>2</sub> Texture

Core diameter = 4"

Imperial Units (1" = 5')



Project/Location:

Logged By:

Date:

Page 9 of 10

Depth	CO <sub>3</sub> Texture					Carb. Classic	Facies	Grains	Sed. Struct.		Grain Size (mm)	Dry Color	Fracture		Photo	Effervescence	Comments
	M	W	P	G	B				Mech.	I.I.			Freq.	Cement			
7680											3/5 PB 15				0		
											2.5/5 PB 15				0		
											15				0		
											15				0		
7685											15				0	Broken up	
											15				0		
							0 ▽				3/5 PB 15				0		
											4/5 PB 15				0		
7690							0				15				0		
											15				0		
											15				0	Broken up	
											15				0		
7695											3/5 PB 15				0		
											2.5/5 PB 20				0	Broken up, Possible TE	
											20				0		
											20				0		
											3/5 PB 20				0		
7700											4/5 10	5 S:Q			0	5mm Aperture Fractures, Qtz Healed in dolo	
											3/5 PB 20				0	Crazy Fracture, Qtz Healed	
							0				20	S:Q			0		
											20				0		
							▽				20				0		
7705											4/5 PB 20				0		
											3/5 PB 20				0		
											20				0		
											20				0		
7710											4/5 PB 20				0		
											3/5 PB 20				0		
											20				0		
											20				0		
7715											4/5 PB 20				0	1" TE → lime	
											20				0		
											20				0		
											20				0		
7720											3/5 PB 20				0		

M V F Md C  
SiO<sub>2</sub> Texture

Core diameter = 4"

Imperial Units (1" = 5')



## REFERENCES

- Adams, J. E., 1962, Foreland Pennsylvanian rocks of Texas and eastern New Mexico, *in* C. C. Branson, ed., *Pennsylvanian System in the United States: AAPG Special Publications 23*, p. 372–384.
- Adams, J. E., 1965, Stratigraphic-tectonic development of Delaware Basin: *AAPG Bulletin*, v. 49, no. 11, p. 2140–2148.
- Adams, J. E., H. Freznel, M. Rhodes, and D. Johnson, 1951, Starved Pennsylvanian Midland Basin: *AAPG Bulletin*, v. 35, no. 12, p. 2600–2607.
- Algeo, T. J., and P. H. Heckel, 2008, The Late Pennsylvanian midcontinent sea of North America: a review: *Palaeogeography, Palaeoclimatology, Palaeoecology*, v. 268, no. 3-4, p. 205–221, doi:10.1016/j.palaeo.2008.03.049.
- Asquith, G. B., 2012, *Fundamentals of Petrophysical Well-Log Interpretation: A Course-Note Collection with Commentary*: Lubbock, Texas, George B. Asquith. 596 p.
- Boardman, D. R., and P. H. Heckel, 1989, Glacial-eustatic sea-level curve for early Late Pennsylvanian sequence in north-central Texas and biostratigraphic correlation with curve for midcontinent North America: *Geology*, v. 17, no. 9, p. 802–805.
- Boardman II, D. R., and J. M. Malinky, 1985, Glacial-eustatic control of Virgilian cyclothems in north central Texas: *American Association of Petroleum Geologists, Southwest Section Meeting Transactions*, p. 13–23.
- Bottjer, D. J., and M. L. Droser, 1991, Ichnofabric and basin analysis: *PALAIOS*, v. 6, no. 3, p. 199–205.
- Bouma, A. H., 1962, *Sedimentology of Some Flysch Deposits: a Graphic Approach to Facies Interpretation*: Amsterdam; New York, Elsevier Publishing Company, 168 p.
- Burnside, R. J., 1959, *Geology of Part of the Horseshoe Atoll in Borden and Howard Counties, Texas*: Washington, US Government Printing Office, 23 p.
- Cardott, B. J., and M. W. Lambert, 1985, Thermal maturation by vitrinite reflectance of Woodford Shale, Anadarko Basin, Oklahoma: *AAPG Bulletin*, v. 69, no. 11, p. 1982–1998.
- Cawood, P. A., and C. Buchan, 2007, Linking accretionary orogenesis with supercontinent assembly: *Earth-Science Reviews*, v. 82, no. 3-4, p. 217–256, doi:10.1016/j.earscirev.2007.03.003.

- Cortez III, M., 2012, Chemostratigraphy, Paleooceanography, and Sequence Stratigraphy of the Pennsylvanian-Permian Section in the Midland Basin, Master's thesis: University of Texas at Arlington, Arlington, Texas, 107 p.
- Crass, B. T., 2015, Petrophysical Lithofacies Modeling of the Cline Shale, West Texas, Master's thesis: Baylor University, Waco, Texas, 78p.
- Cummins, W. F., 1891, Report on the geology of northwestern Texas, Part II, Economic Geology, *in* Second Annual Report of the Geological Survey of Texas: Annual Report of the Geological Survey of Texas, p. 357–552.
- Davis, H. R., C. W. Byers, and L. M. Pratt, 1989, Depositional mechanisms and organic matter in Mowry Shale (Cretaceous), Wyoming: AAPG Bulletin, v. 73, no. 9, p. 1103–1116.
- Doveton, J. H., 1994, Neutron-density porosity overlay case studies, *in* Y. K. Bentor, ed., Geological Log Interpretation: Tulsa, Oklahoma, SEPM Special Publication 29, p. 77–90.
- Droser, M. L., and D. J. Bottjer, 1986, A semiquantitative field classification of ichnofabric: Journal of Sedimentary Research, v. 56, no. 4, p. 558–559.
- Dunham, R. J., 1962, Classification of carbonate rocks according to depositional texture, *in* W. E. Ham, ed., Classification of Carbonate Rocks - a Symposium: American Association of Petroleum Geologists, AAPG Memoir 1, p. 108–121.
- Dutton, S. P., E. M. Kim, R. F. Broadhead, W. D. Raatz, C. L. Breton, S. C. Ruppel, and C. Kerans, 2005, Play analysis and leading-edge oil-reservoir development methods in the Permian Basin: increased recovery through advanced technologies: AAPG Bulletin, v. 89, no. 5, p. 553–576.
- Embry III, A. F., and J. E. Klovan, 1971, A Late Devonian reef tract on Northeastern Banks Island, N.W.T.: Bulletin of Canadian Petroleum Geology, v. 19, no. 4, p. 730–781.
- Enos, P., and C. H. Moore, 1983, Fore reef slope environment: Chapter 10, *in* P. A. Scholle, D. G. Bebout, and C. H. Moore, eds., Carbonate Depositional Environment: AAPG Memoir 33, p. 507–537.
- Galley, J. E., 1958, Oil and geology in the Permian Basin of Texas and New Mexico, *in* L. G. Weeks, ed., Habitat of Oil: AAPG Special Volumes 18, p. 395–446.
- Galloway, W. E., and L. F. Brown Jr, 1973, Depositional systems and shelf-slope relations on cratonic basin margin, uppermost Pennsylvanian of north-central Texas: AAPG Bulletin, v. 57, no. 7, p. 1185–1218.

- Greenlee, S. M., and P. J. Lehmann, 1993, Stratigraphic framework of productive carbonate buildups: chapter 2, *in* R. G. Loucks, and J. F. Sarg, eds., Carbonate Sequence Stratigraphy: Recent Developments and Applications: AAPG Memoir 57, p. 43–62.
- Heckel, P. H., 1977, Origin of phosphatic black shale facies in Pennsylvanian cyclothems of mid-continent North America: AAPG Bulletin, v. 61, no. 7, p. 1045–1068.
- Heck, W. A., K. A. Yenne, and L. G. Henbest, 1952, Boundary of Pennsylvanian and Permian (?) in the Subsurface Scurry Reef, Scurry County, Texas, Report of Investigations 13: Austin, Bureau of Economic Geology The University of Texas, 16 p.
- Hickey, J. J., and B. Henk, 2007, Lithofacies summary of the Mississippian Barnett Shale, Mitchell 2 T.P. Sims well, Wise County, Texas: AAPG Bulletin, v. 91, no. 4, p. 437–443, doi:10.1306/12040606053.
- Hills, J. M., 1972, Late Paleozoic sedimentation in west Texas Permian Basin: AAPG Bulletin, v. 56, no. 12, p. 2303–2322.
- Hobson, J. P., C. D. Caldwell, and D. F. Toomey, 1985a, Early Permian deep-water allochthonous limestone facies and reservoir, west Texas: AAPG Bulletin, v. 69, no. 12, p. 2130–2147.
- Hobson, J. P., C. D. Caldwell, and D. F. Toomey, 1985b, Sedimentary facies and biota of Early Permian deep-water allochthonous limestone, southwest Reagan County, Texas, *in* Deep-Water Carbonates: Buildups, Turbidites, Debris Flows, and Chalks: SEPM Core Workshop 6, p. 93–139.
- Ibach, L. E. J., 1982, Relationship between sedimentation rate and total organic carbon content in ancient marine sediments: AAPG Bulletin, v. 66, no. 2, p. 170–188.
- Kinley, T. J., L. W. Cook, J. A. Breyer, D. M. Jarvie, and A. B. Busbey, 2008, Hydrocarbon potential of the Barnett Shale (Mississippian), Delaware Basin, west Texas and southeastern New Mexico: AAPG Bulletin, v. 92, no. 8, p. 967–991, doi:10.1306/03240807121.
- Kohl, D., R. Slingerland, M. Arthur, R. Bracht, and T. Engelder, 2014, Sequence stratigraphy and depositional environments of the Shamokin (Union Springs) Member, Marcellus Formation, and associated strata in the middle Appalachian Basin: AAPG Bulletin, v. 98, no. 3, p. 483–513, doi:10.1306/08231312124.
- Landing, E., 2012, The great American carbonate bank in eastern Laurentia: its births, deaths, and linkage to paleoceanic oxygenation (Early Cambrian–Late Ordovician): The great American carbonate bank: The geology and economic resources of the Cambrian-Ordovician Sauk megasequence of Laurentia: AAPG Memoir, v. 98, p. 451–492.

- Lash, G. G., and D. R. Blood, 2014, Organic matter accumulation, redox, and diagenetic history of the Marcellus Formation, southwestern Pennsylvania, Appalachian basin: *Marine and Petroleum Geology*, v. 57, p. 244–263, doi:10.1016/j.marpetgeo.2014.06.001.
- Martin, H., 2012, Devon energy overview: the company, exploration, and technology: Tulsa Geological Society Meeting, Tulsa Oklahoma, AAPG Search and Discovery Article #70124.
- Mazzullo, L. J., and S. J. Mazzullo, 1983, Atoll reservoir facies in Pennsylvanian limestone Higgins Ranch field, Coke County, Texas, *in* P. M. Harris, ed.: SEPM Society for Sedimentary Geology, SEPM Core Workshop Notes, p. 223–243.
- Mazzullo, S. J., and A. M. Reid, 1989, Lower Permian platform and basin depositional systems, northern Midland Basin, Texas, *in* P. Crevello, J. L. Wilson, J. F. Sarg, and J. F. Read, eds., *Controls on Carbonate Platform and Basin Development*: SEPM Special Publication 44, p. 305–320.
- Mertz Jr, K. A., 1989, Origin of hemipelagic source rocks during early and middle Miocene, Monterey Formation, Salinas Basin, California: *AAPG Bulletin*, v. 73, no. 4, p. 510–524.
- Miceli Romero, A., and R. P. Philip, 2012, Organic geochemistry of the Woodford Shale, southeastern Oklahoma: How variable can shales be? *AAPG Bulletin*, v. 96, no. 3, p. 493–517, doi:10.1306/08101110194.
- Myers, D. A., P. T. Stafford, and R. J. Burnside, 1957, *Geology of the Late Paleozoic Horseshoe Atoll, West Texas*.
- Passey, Q. R., S. Creaney, J. B. Kulla, F. J. Moretti, and J. D. Stroud, 1990, A practical model for organic richness from porosity and resistivity logs: *American Association of Petroleum Geologists Bulletin*, v. 74, no. 12, p. 1777–1794.
- Pollastro, R. M., D. M. Jarvie, R. J. Hill, and C. W. Adams, 2007, Geologic framework of the Mississippian Barnett Shale, Barnett-Paleozoic total petroleum system, Bend Arch–Fort Worth Basin, Texas: *AAPG Bulletin*, v. 91, no. 4, p. 405–436, doi:10.1306/10300606008.
- Reid, A. M., and S. Tomlinson-Reid, 1991, The Cogdell field study, Kent and Scurry Counties, Texas: a post mortem, *in* M. Candelaria, ed., *Tomorrow's Technology Today*: West Texas Geology Society Symposium, Pub. No. 91-89, p. 39–66.
- Ross, C. A., and J. R. P. Ross, 1987, Late Paleozoic sea levels and depositional sequences, *in* C. A. Ross, and D. Haman, eds., *Timing and Depositional History of Eustatic Sequences, Constraints on Seismic Stratigraphy*: Ithaca, New York, Cushman Foundation for Foraminiferal Research, v. 24, p. 137–149.

- Ross, C. A., and J. R. P. Ross, 1988, Late Paleozoic transgressive-regressive deposition, *in* C. K. Wilgus, B. S. Hastings, C. G. Kendall, H. W. Posamentier, C. A. Ross, and J. C. Van Wagoner, eds., *Sea-Level Changes - an Integrated Approach*: Society for Sedimentary Geology (SEPM) Special Publication 42, p. 227–247.
- Saller, A. H., J. A. D. Dickson, and S. A. Boyd, 1994, Cycle stratigraphy and porosity in Pennsylvanian and lower Permian shelf limestones, eastern Central Basin Platform, Texas: *AAPG Bulletin*, v. 78, no. 12, p. 1820–1842.
- Sarg, J. F., J. R. Markello, and L. J. Weber, 1999, The second-order cycle, carbonate-platform growth, and reservoir, source, and trap prediction, *in* P. M. Harris, A. H. Saller, and J. A. Simo, eds., *Advances in Carbonate Sequence Stratigraphy: Application to Reservoirs, Outcrops, and Models*: SEPM Special Publication 63, p. 11–34.
- Schatzinger, R. A., 1987, Depositional environments and diagenesis of the eastern portion of the Horseshoe Atoll, West Texas, Ph.D. dissertation: The University of Texas at Austin, Austin, Texas, 340 p.
- Schlager, W., 1992, Accommodation and sediment supply; a dual control on stratigraphic sequences, *in* T. Simo, E. Franseen, and M. Harris, eds., *Carbonate Stratigraphic Sequences; Sequence Boundaries and Associated Facies (emphasis on Outcrop and Process Studies)*: Society of Economic Paleontologists and Mineralogists/International Association of Sedimentologists, Spain, 93 p.
- Schmoker, J. W., and T. C. Hester, 1983, Organic carbon in Bakken Formation, United States portion of Williston Basin: *AAPG Bulletin*, v. 67, no. 12, p. 2165–2174.
- Shanmugam, G., 1997, The Bouma Sequence and the turbidite mind set: *Earth-Science Reviews*, v. 42, no. 4, p. 201–229.
- Stampfli, G. M., C. Hochard, C. V  rard, C. Wilhem, and J. vonRaumer, 2013, The formation of Pangea: *Tectonophysics*, v. 593, no. 0, p. 1–19, doi:10.1016/j.tecto.2013.02.037.
- Tai, P. C., 2001, Late Paleozoic Foreland Deformation in the Southwestern Midland Basin and Adjacent Areas: Implications for Tectonic Evolution of the Permian Basin, West Texas, Ph.D. dissertation: Texas A & M University, College Station, Texas, 193 p.
- Tyson, R. V., 2001, Sedimentation rate, dilution, preservation and total organic carbon: some results of a modelling study: *Organic Geochemistry*, v. 32, no. 2, p. 333–339, doi:10.1016/S0146-6380(00)00161-3.
- Vest Jr., E. L., 1970, Oil fields of Pennsylvanian-Permian Horseshoe Atoll, west Texas, *in* M. T. Halbouty, ed., *Geology of Giant Petroleum Fields*: AAPG Memoir 14, p. 185–203.

- Waite, L. E., 1993, Upper Pennsylvanian seismic sequences and facies of the eastern and southern Horseshoe Atoll, Midland Basin, west Texas, *in* R. G. Loucks, and J. F. Sarg, eds., Carbonate Sequence Stratigraphy: Recent Developments and Applications: AAPG Memoir 57, p. 210–240.
- Walker, D. A., J. Golonka, A. Reid, and S. Reid, 1995, The effects of paleolatitude and paleogeography on carbonate sedimentation in the late Paleozoic: AAPG Special Volumes, v. 40, no. Paleogeography, Paleoclimate, and Source Rocks, p. 133–155.
- Wang, G., and T. R. Carr, 2013, Prediction and Distribution Analysis of Marcellus Shale Productive Facies in the Appalachian Basin, USA, Oral Presentation: AAPG Annual Convention and Exhibition, Pittsburgh, Pennsylvania, AAPG Search and Discovery Article #80319.
- Wright, W. R., 2011a, Depositional History of the Desmoinesian Succession (Middle Pennsylvanian) in the Midland Basin, Unpublished thesis: Bureau of Economic Geology, Jackson School of Geosciences, The University of Texas at Austin, Austin, Texas, 97 p.
- Wright, W. R., 2011b, Pennsylvanian paleodepositional evolution of the greater Permian Basin, Texas and New Mexico: depositional systems and hydrocarbon reservoir analysis: AAPG Bulletin, v. 95, no. 9, p. 1525–1555.
- Yancey, T. E., 1986, Controls on the deposition of mixed carbonate and siliciclastic sediments on the Eastern Shelf of the Midland Basin, Pennsylvanian of Texas: Gulf Coast Association of Geological Societies, v. 36, p. 361–366.
- Yang, K. M., and S. L. Dorobek, 1995, The Permian Basin of west Texas and New Mexico: tectonic history of a “composite” foreland basin and its effects on stratigraphic development, *in* S. L. Dorobek, and G. M. Ross, eds., Stratigraphic Evolution of Foreland Basins: SEPM Special Publication 52, p. 149–174.
- Yang, W., and M. A. Kominz, 2003, Characteristics, stratigraphic architecture, and time framework of multi-order mixed siliciclastic and carbonate depositional sequences, outcropping Cisco group (late Pennsylvanian and early Permian), Eastern Shelf, north-central Texas, USA: Sedimentary Geology, v. 154, p. 53–87.